Chapter 13
Path-following of Underactuated Underwater Vehicles

This chapter extends the approach proposed for underactuated surface ships in Chapter 11 to design a path-following system for six degrees of freedom underactuated underwater vehicles. Although the control design is much more involved in comparison with that for underactuated surface ships in Chapter 11, it still guarantees that path-following errors asymptotically converge to a ball, with an adjustable radius, centered on a desired path, and covers both parking and point-to-point navigation problems.

13.1 Control Objective

For the reader's convenience, we rewrite the mathematical model of an underactuated underwater vehicle, which is described in detail in Section 3.4.2.1, moving in six degrees of freedom as follows:

$$\begin{aligned}
&\dot{\boldsymbol{\eta}}_{\mathbf{1}} = \boldsymbol{J}_{\mathbf{1}}(\boldsymbol{\eta}_{\mathbf{2}})\boldsymbol{v}_{\mathbf{1}},\\
&\boldsymbol{M}_{\mathbf{1}}\dot{\boldsymbol{v}}_{\mathbf{1}} = -\boldsymbol{C}_{\mathbf{1}}(\boldsymbol{v}_{\mathbf{1}})\boldsymbol{v}_{\mathbf{2}} - \boldsymbol{D}_{\mathbf{1}}\boldsymbol{v}_{\mathbf{1}} - \boldsymbol{D}_{\boldsymbol{n}\mathbf{1}}(\boldsymbol{v}_{\mathbf{1}})\boldsymbol{v}_{\mathbf{1}} + \boldsymbol{\tau}_{\mathbf{1}} + \boldsymbol{\tau}_{\mathbf{1}\boldsymbol{E}},\\
&\dot{\boldsymbol{\eta}}_{\mathbf{2}} = \boldsymbol{J}_{\mathbf{2}}(\boldsymbol{\eta}_{\mathbf{2}})\boldsymbol{v}_{\mathbf{2}},\\
&\boldsymbol{M}_{\mathbf{2}}\dot{\boldsymbol{v}}_{\mathbf{2}} = -\boldsymbol{C}_{\mathbf{1}}(\boldsymbol{v}_{\mathbf{1}})\boldsymbol{v}_{\mathbf{1}} - \boldsymbol{C}_{\mathbf{2}}(\boldsymbol{v}_{\mathbf{2}})\boldsymbol{v}_{\mathbf{2}} - \boldsymbol{D}_{\mathbf{2}}\boldsymbol{v}_{\mathbf{2}} - \boldsymbol{D}_{\boldsymbol{n}\mathbf{2}}(\boldsymbol{v}_{\mathbf{2}})\boldsymbol{v}_{\mathbf{2}} -\\
&\qquad\qquad \boldsymbol{g}_{\mathbf{2}}(\boldsymbol{\eta}_{\mathbf{2}}) + \boldsymbol{\tau}_{\mathbf{2}} + \boldsymbol{\tau}_{\mathbf{2}\boldsymbol{E}},
\end{aligned} \tag{13.1}$$

where $\boldsymbol{J}_{\mathbf{1}}(\boldsymbol{\eta}_{\mathbf{2}})$ and $\boldsymbol{J}_{\mathbf{2}}(\boldsymbol{\eta}_{\mathbf{2}})$ are given by

$$\boldsymbol{J}_{\mathbf{1}}(\boldsymbol{\eta}_{\mathbf{2}}) = \begin{bmatrix}
\cos(\psi)\cos(\theta) & -\sin(\psi)\cos(\phi) + \sin(\phi)\sin(\theta)\cos(\psi) & \sin(\psi)\sin(\phi) + \sin(\theta)\cos(\psi)\cos(\phi)\\
\sin(\psi)\cos(\theta) & \cos(\psi)\cos(\phi) + \sin(\phi)\sin(\theta)\sin(\psi) & -\cos(\psi)\sin(\phi) + \sin(\theta)\sin(\psi)\cos(\phi)\\
-\sin(\theta) & \sin(\phi)\cos(\theta) & \cos(\phi)\cos(\theta)
\end{bmatrix},$$

$$\boldsymbol{J_2}(\boldsymbol{\eta_2}) = \begin{bmatrix} 1 & \sin(\phi)\tan(\theta) & \cos(\phi)\tan(\theta) \\ 0 & \cos(\phi) & -\sin(\phi) \\ 0 & \sin(\phi)/\cos(\theta) & \cos(\phi)/\cos(\theta) \end{bmatrix}. \tag{13.2}$$

The matrices $\boldsymbol{M_1}$ and $\boldsymbol{M_2}$ are

$$\boldsymbol{M_1} = \begin{bmatrix} m_{11} & 0 & 0 \\ 0 & m_{22} & 0 \\ 0 & 0 & m_{33} \end{bmatrix}, \boldsymbol{M_2} = \begin{bmatrix} m_{44} & 0 & 0 \\ 0 & m_{55} & 0 \\ 0 & 0 & m_{66} \end{bmatrix}. \tag{13.3}$$

The matrices $\boldsymbol{C_1}(\boldsymbol{v_1})$ and $\boldsymbol{C_2}(\boldsymbol{v_2})$ are

$$\begin{aligned} \boldsymbol{C_1}(\boldsymbol{v_1}) &= \begin{bmatrix} 0 & m_{33}w & -m_{22}v \\ -m_{33}w & 0 & m_{11}u \\ m_{22}v & -m_{11}u & 0 \end{bmatrix}, \\ \boldsymbol{C_2}(\boldsymbol{v_2}) &= \begin{bmatrix} 0 & m_{66}r & -m_{55}q \\ -m_{66}r & 0 & m_{44}p \\ m_{55}q & -m_{44}p & 0 \end{bmatrix}. \end{aligned} \tag{13.4}$$

The linear and nonlinear damping matrices $\boldsymbol{D_1}$, $\boldsymbol{D_2}$, $\boldsymbol{D_{n1}}(\boldsymbol{v_1})$, and $\boldsymbol{D_{n2}}(\boldsymbol{v_2})$ are

$$\begin{aligned} \boldsymbol{D_1} &= \begin{bmatrix} d_{11} & 0 & 0 \\ 0 & d_{22} & 0 \\ 0 & 0 & d_{33} \end{bmatrix}, \boldsymbol{D_2} = \begin{bmatrix} d_{44} & 0 & 0 \\ 0 & d_{55} & 0 \\ 0 & 0 & d_{66} \end{bmatrix}, \\ \boldsymbol{D_{n1}}(\boldsymbol{v_1}) &= \begin{bmatrix} \sum_{i=2}^{3} d_{ui}|u|^{i-1} & 0 & 0 \\ 0 & \sum_{i=2}^{3} d_{vi}|v|^{i-1} & 0 \\ 0 & 0 & \sum_{i=2}^{3} d_{wi}|w|^{i-1} \end{bmatrix}, \\ \boldsymbol{D_{n2}}(\boldsymbol{v_2}) &= \begin{bmatrix} \sum_{i=2}^{3} d_{pi}|p|^{i-1} & 0 & 0 \\ 0 & \sum_{i=2}^{3} d_{qi}|q|^{i-1} & 0 \\ 0 & 0 & \sum_{i=2}^{3} d_{ri}|r|^{i-1} \end{bmatrix}. \end{aligned} \tag{13.5}$$

The restoring force and moment vector $\boldsymbol{g_2}(\boldsymbol{\eta_2})$ is given by

$$\boldsymbol{g_2}(\boldsymbol{\eta_2}) = \begin{bmatrix} \rho g \nabla \overline{GM_T} \sin(\phi)\cos(\theta) \\ \rho g \nabla \overline{GM_L} \sin(\theta) \\ 0 \end{bmatrix}. \tag{13.6}$$

The propulsion force and moment vectors $\boldsymbol{\tau_1}$ and $\boldsymbol{\tau_2}$ are

$$\boldsymbol{\tau_1} = \begin{bmatrix} \tau_u \\ 0 \\ 0 \end{bmatrix}, \quad \boldsymbol{\tau_2} = \begin{bmatrix} \tau_p \\ \tau_q \\ \tau_r \end{bmatrix}, \tag{13.7}$$

which imply that the vehicle under consideration does not have independent actuators in the sway and heave. The environmental disturbance vectors $\boldsymbol{\tau_{1E}}$ and $\boldsymbol{\tau_{2E}}$

are given by

$$\boldsymbol{\tau_{1E}} = \begin{bmatrix} \tau_{Eu}(t) \\ \tau_{Ev}(t) \\ \tau_{Ew}(t) \end{bmatrix}, \boldsymbol{\tau_{2E}} = \begin{bmatrix} \tau_{Ep}(t) \\ \tau_{Eq}(t) \\ \tau_{Er}(t) \end{bmatrix}, \tag{13.8}$$

where $\tau_{Eu}(t)$, $\tau_{Ev}(t)$, $\tau_{Ew}(t)$, $\tau_{Ep}(t)$, $\tau_{Eq}(t)$, and $\tau_{Er}(t)$ are the environmental disturbance forces or moments acting on the surge, sway, heave, roll, pitch, and yaw axes, respectively.

We assume that these disturbances are bounded as follows:

$$\begin{aligned} &|\tau_{Eu}(t)| \le \tau_{Eu}^{\max} < \infty, |\tau_{Ev}(t)| \le \tau_{Ev}^{\max} < \infty, |\tau_{Ew}(t)| \le \tau_{Ew}^{\max} < \infty, \\ &\left|\tau_{Ep}(t)\right| \le \tau_{Ep}^{\max} < \infty, \left|\tau_{Eq}(t)\right| \le \tau_{Eq}^{\max} < \infty, |\tau_{Er}(t)| \le \tau_{Er}^{\max} < \infty. \end{aligned} \tag{13.9}$$

Since the sway and heave control forces are not available in the sway and heave dynamics, the vehicle model (13.1) is underactuated.

In this chapter, we consider a control objective of designing the control inputs $\boldsymbol{\tau_1}$ and $\boldsymbol{\tau_2}$ to force the underactuated vehicle (13.1) to follow a specified path $\boldsymbol{\Omega}$, see Figure 13.1. If we are able to drive the vehicle to follow closely a virtual vessel that moves along the path with a desired speed u_0, then the control objective is fulfilled, i.e., the vessel is in a tube of nonzero diameter centered on the reference path and moves along the specified path at the speed u_0. Roughly speaking, the approach is to steer the vessel such that it heads toward the virtual one and diminishes the distance between the real and the virtual vessels.

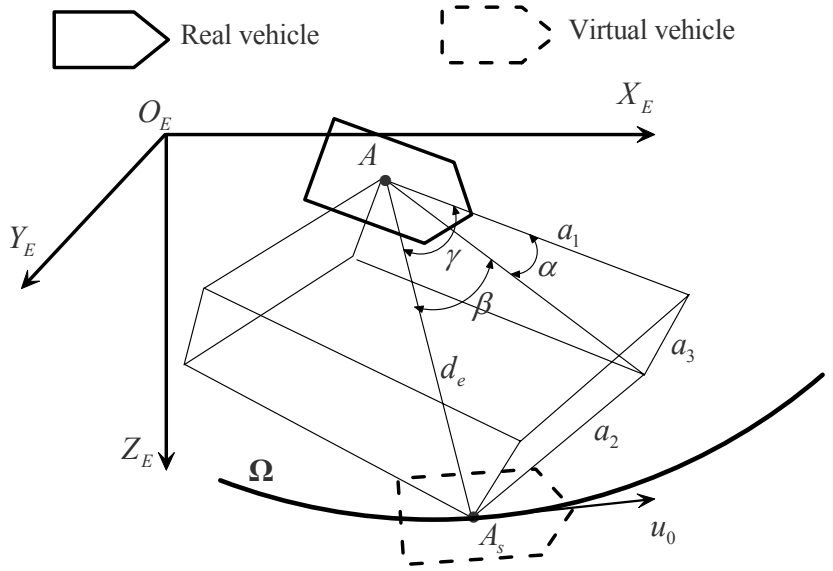

Figure 13.1 General framework of underwater vehicle path-following

In Figure 13.1, A is the center of the real vehicle and A_s is a point on the reference path attached to the virtual vehicle. Define the following path-following errors

$$\begin{aligned} x_e &= x_d - x, \\ y_e &= y_d - y, \\ z_e &= z_d - z, \\ d_e &= \sqrt{x_e^2 + y_e^2 + z_e^2}, \end{aligned} \tag{13.10}$$

where x_d, y_d and z_d are the coordinates of A_s. Then the terms $a_i, 1 \leq i \leq 3$ in Figure 13.1 are obtained from x_e, y_e and z_e by rotating the body frame around the earth-fixed frame $O_E X_E Y_E Z_E$ the roll, pitch, and yaw angles, i.e.,

$$\begin{bmatrix} a_1 \\ a_2 \\ a_3 \end{bmatrix} = \boldsymbol{J_1}(\boldsymbol{\eta_2}) \begin{bmatrix} x_e \\ y_e \\ z_e \end{bmatrix}. \tag{13.11}$$

Expanding (13.11) yields

$$\begin{aligned} a_1 &= x_e J_1^{11}(\boldsymbol{\eta_2}) + y_e J_1^{21}(\boldsymbol{\eta_2}) + z_e J_1^{31}(\boldsymbol{\eta_2}), \\ a_2 &= x_e J_1^{12}(\boldsymbol{\eta_2}) + y_e J_1^{22}(\boldsymbol{\eta_2}) + z_e J_1^{32}(\boldsymbol{\eta_2}), \\ a_3 &= x_e J_1^{13}(\boldsymbol{\eta_2}) + y_e J_1^{23}(\boldsymbol{\eta_2}) + z_e J_1^{33}(\boldsymbol{\eta_2}), \end{aligned} \tag{13.12}$$

where $J_1^{ij}(\eta_2)$ is the element of $\boldsymbol{J_1}(\boldsymbol{\eta_2})$ at the ith row and jth column. Therefore the path-following orientation errors are defined by the angles α and β. It is noted that the angles γ, α, and β are not defined at $d_e = 0$ but with the aid of a desired controller, $\lim_{\|(d_e,\alpha,\beta)\| \to 0}(\theta, \psi) = (\theta_s, \psi_s)$ with θ_s and ψ_s being the orientation angles of the virtual vessel. Hence in this chapter, we will design a controller such that it guarantees $d_e \geq d_e^*$ with d_e^* being an arbitrarily small positive constant to avoid chattering caused by $d_e = 0$. With the above definitions, our control objective can be mathematically stated as follows:

Path-following Objective. Under Assumption 13.1, design the control inputs $\boldsymbol{\tau_1}$ and $\boldsymbol{\tau_2}$ to force the underactuated vehicle (13.1) to follow the path $\boldsymbol{\Omega}$ given by

$$\begin{aligned} x_d &= x_d(s), \\ y_d &= y_d(s), \\ z_d &= z_d(s), \end{aligned} \tag{13.13}$$

where s is the path parameter variable, such that

$$\begin{aligned} &\lim_{t \to \infty} d_e(t) \leq \overline{d_e}, \ \lim_{t \to \infty} |\alpha(t)| \leq \overline{\alpha}, \\ &\lim_{t \to \infty} |\beta(t)| \leq \overline{\beta}, \ \lim_{t \to \infty} |\phi(t)| \leq \overline{\phi}, \end{aligned}$$

with $\overline{d_e}$, $\overline{\phi}$, $\overline{\alpha}$, and $\overline{\beta}$ being arbitrarily small positive constants.

Assumption 13.1. *The reference path is regular, i.e. there exist strictly positive constants* $a_{3\min}, a_{3\max}, a_{2\min}$ *and* $a_{2\max}$ *such that*

$$a_{3\min} \leq \sqrt{\left(\frac{\partial x_d}{\partial s}\right)^2 + \left(\frac{\partial y_d}{\partial s}\right)^2 + \left(\frac{\partial z_d}{\partial s}\right)^2} \leq a_{3\max},$$
$$a_{2\min} \leq \sqrt{\left(\frac{\partial x_d}{\partial s}\right)^2 + \left(\frac{\partial y_d}{\partial s}\right)^2} \leq a_{2\max}. \tag{13.14}$$

Remark 13.1.

1. We might refer to the above objective as a path-tracking one. However, we use the term "path-following" since our approach is to make the real vehicle follow the virtual one, see Figure 13.1.
2. Assumption 13.1 ensures that the path is feasible for the vessel to follow, see Section 13.3. The condition (13.14) implies that the reference trajectory cannot contain a vertical straight line to avoid singularity of $\boldsymbol{J_2(\eta_2)}$ at the pitch angle $\theta = \pm 0.5\pi$.
3. If the reference path is not regular, then we can often split it into regular pieces and consider each of them separately. This is the case of point-to-point navigation, which will be addressed in Section 13.6.
4. The path parameter, s, is not the arc length of the path in general. For example, a circle with radius R centered at the origin can be described as $x_d = R\cos(s)$ and $y_d = R\sin(s)$.

13.2 Coordinate Transformations

From (13.10) and (13.12), we have the position kinematic error dynamics as follows:

$$\dot{d}_e = \frac{1}{d_e}\left(x_e\frac{\partial x_d}{\partial s} + y_e\frac{\partial y_d}{\partial s} + z_e\frac{\partial z_d}{\partial s}\right)\dot{s} - \frac{a_1}{d_e}u - \frac{a_2}{d_e}v - \frac{a_3}{d_e}w. \tag{13.15}$$

For the path-following orientation errors, referring to Figure 13.1 and the control objective stated in the previous section, one can see that the following holds

$$\frac{a_1}{d_e} = \cos(\gamma) = \cos(\alpha)\cos(\beta), \tag{13.16}$$

which in turn implies that

$$\begin{cases} \lim\limits_{t\to\infty} \alpha(t) = 0 \\ \lim\limits_{t\to\infty} \beta(t) = 0 \end{cases} \Leftrightarrow \lim_{t\to\infty} \gamma(t) = 0 \Rightarrow \lim_{t\to\infty}\left(\frac{a_1(t)}{d_e(t)}\right) = 1. \tag{13.17}$$

Hence we can either choose the angles α and β, or the angle γ, or the term a_1/d_e as the orientation coordinates for the control design. We now discuss the above options and then choose one that results in a simple control design and enhance feasible initial conditions.

Using Angles α and β. In this case, the path-following orientation errors are defined as follows, see Figure 13.1:

$$\begin{aligned} \alpha &= e_\alpha - 2\pi n_\alpha(e_\alpha), \\ \beta &= e_\beta - 2\pi n_\beta(e_\beta), \end{aligned} \tag{13.18}$$

where

$$e_\alpha = \begin{cases} 2\arctan\left(\dfrac{a_3}{a_1}\right);\ (a_3,a_1) \neq (0,0), \\ 0;\ (a_3,a_1) = (0,0), \end{cases}$$

$$e_\beta = \begin{cases} 2\arctan\left(\dfrac{a_2}{\sqrt{a_1^2+a_3^2}}\right);\ \left(a_2, \sqrt{a_1^2+a_3^2}\right) \neq (0,0), \\ 0\ \ ;\ \left(a_2, \sqrt{a_1^2+a_3^2}\right) = (0,0). \end{cases} \tag{13.19}$$

The functions $n_\alpha(e_\alpha)$ and $n_\beta(e_\beta)$ take values in $(0, \pm 1, \pm 2, ...)$ such that α and β belong to $(-\pi, \pi]$. Hence α and β are periodic and piecewise continuous functions with respect to e_α and e_β. The reason for introducing (13.18) is to convert all equilibrium points of α and β to the origin. It is seen from (13.19) that e_α and e_β are discontinuous on the following surfaces:

$$\begin{aligned} D_\alpha &= \{(a_1,a_3) : a_3 \neq 0, a_1 = 0\}, \\ D_\beta &= \left\{(a_1,a_2,a_3) : a_2 \neq 0, \sqrt{a_1^2+a_3^2} = 0\right\}. \end{aligned} \tag{13.20}$$

It is also seen from (13.18) that α and β are discontinuous on the surfaces:

$$\begin{aligned} C_\alpha &= \{(a_1,a_3) : \alpha = \pi\}, \\ C_\beta &= \{(a_1,a_2,a_3) : \beta = \pi\}. \end{aligned} \tag{13.21}$$

We now use (13.18) to transform the kinematic part of (13.1) to

$$\dot{\boldsymbol{\eta}}_{\boldsymbol{\alpha\beta}} = \boldsymbol{f}^{\boldsymbol{s}}_{\boldsymbol{\alpha\beta}}(\cdot)\dot{s} + \boldsymbol{f}^{\boldsymbol{u}}_{\boldsymbol{\alpha\beta}}(\cdot)u + \boldsymbol{f}^{\boldsymbol{v}}_{\boldsymbol{\alpha\beta}}(\cdot)v + \boldsymbol{f}^{\boldsymbol{w}}_{\boldsymbol{\alpha\beta}}(\cdot)w + \boldsymbol{A}_{\boldsymbol{\alpha\beta}}(\cdot)\boldsymbol{J}_{\boldsymbol{2}}(\boldsymbol{\eta}_{\boldsymbol{2}})\boldsymbol{v}_{\boldsymbol{2}}, \tag{13.22}$$

where

$$\begin{aligned} \boldsymbol{\eta}_{\boldsymbol{\alpha\beta}} &= \begin{bmatrix} \phi & \alpha & \beta \end{bmatrix}^T, \\ \boldsymbol{f}^{\boldsymbol{s}}_{\boldsymbol{\alpha\beta}}(\cdot) &= \boldsymbol{F}_{\boldsymbol{\alpha\beta}}(\cdot)\begin{bmatrix} \dfrac{\partial x_d}{\partial s} & \dfrac{\partial y_d}{\partial s} & \dfrac{\partial z_d}{\partial s} \end{bmatrix}^T, \end{aligned}$$

$$
\begin{aligned}
\boldsymbol{f}^{\boldsymbol{u}}_{\boldsymbol{\alpha\beta}}(\cdot) &= -\boldsymbol{F}_{\boldsymbol{\alpha\beta}}(\cdot)\left[\, J_1^{11}(\boldsymbol{\eta_2})\ J_1^{21}(\boldsymbol{\eta_2})\ J_1^{31}(\boldsymbol{\eta_2})\,\right]^T,\\
\boldsymbol{f}^{\boldsymbol{v}}_{\boldsymbol{\alpha\beta}}(\cdot) &= -\boldsymbol{F}_{\boldsymbol{\alpha\beta}}(\cdot)\left[\, J_1^{12}(\boldsymbol{\eta_2})\ J_1^{22}(\boldsymbol{\eta_2})\ J_1^{32}(\boldsymbol{\eta_2})\,\right]^T,\\
\boldsymbol{f}^{\boldsymbol{w}}_{\boldsymbol{\alpha\beta}}(\cdot) &= -\boldsymbol{F}_{\boldsymbol{\alpha\beta}}(\cdot)\left[\, J_1^{13}(\boldsymbol{\eta_2})\ J_1^{23}(\boldsymbol{\eta_2})\ J_1^{33}(\boldsymbol{\eta_2})\,\right]^T,\\
\boldsymbol{F}_{\boldsymbol{\alpha\beta}}(\cdot) &= \left[\, 0\ \boldsymbol{f}^{\boldsymbol{1}}_{\boldsymbol{\alpha\beta}}(\cdot)\ \boldsymbol{f}^{\boldsymbol{2}}_{\boldsymbol{\alpha\beta}}(\cdot)\,\right]^T,\\
\boldsymbol{A}_{\boldsymbol{\alpha\beta}}(\cdot) &= \begin{bmatrix} 1 & 0 \\ -\cos(\alpha)\tan(\beta)\ \cos(\phi)+\sin(\alpha)\tan(\beta)\sin(\phi) & \\ \sin(\alpha) & \sin(\phi)\cos(\alpha) \end{bmatrix}\\
&\qquad \begin{bmatrix} 0 \\ \cos(\theta)\sin(\phi)+\tan(\beta)(\sin(\theta)\cos(\alpha)-\cos(\theta)\sin(\alpha)\cos(\phi) \\ -(\cos(\alpha)\cos(\theta)\cos(\phi)+\sin(\alpha)\sin(\theta) \end{bmatrix},
\end{aligned}
\tag{13.23}
$$

with

$$
\begin{aligned}
\boldsymbol{f}^{\boldsymbol{1}}_{\boldsymbol{\alpha\beta}}(\cdot) = \ & \frac{1}{d_e\cos(\beta)}\big[\cos(\alpha)J_1^{13}(\boldsymbol{\eta_2})-\sin(\alpha)J_1^{11}(\boldsymbol{\eta_2}),\\
& \cos(\alpha)J_1^{23}(\boldsymbol{\eta_2})-\sin(\alpha)J_1^{21}(\boldsymbol{\eta_2}),\\
& \cos(\alpha)J_1^{33}(\boldsymbol{\eta_2})-\sin(\alpha)J_1^{31}(\boldsymbol{\eta_2})\big],\\
\boldsymbol{f}^{\boldsymbol{2}}_{\boldsymbol{\alpha\beta}}(\cdot) = \ & \Big[-\frac{\sin(\beta)\cos(\alpha)}{d_e}J_1^{11}(\boldsymbol{\eta_2})+\frac{\cos(\beta)}{d_e}J_1^{12}(\boldsymbol{\eta_2})-\frac{\sin(\beta)\sin(\alpha)}{d_e}J_1^{13}(\boldsymbol{\eta_2}),\\
& -\frac{\sin(\beta)\cos(\alpha)}{d_e}J_1^{21}(\boldsymbol{\eta_2})+\frac{\cos(\beta)}{d_e}J_1^{22}(\boldsymbol{\eta_2})-\frac{\sin(\beta)\sin(\alpha)}{d_e}J_1^{23}(\boldsymbol{\eta_2}),\\
& -\frac{\sin(\beta)\cos(\alpha)}{d_e}J_1^{31}(\boldsymbol{\eta_2})+\frac{\cos(\beta)}{d_e}J_1^{32}(\boldsymbol{\eta_2})-\frac{\sin(\beta)\sin(\alpha)}{d_e}J_1^{33}(\boldsymbol{\eta_2})\Big].
\end{aligned}
\tag{13.24}
$$

From (13.23), we calculate the determination of the matrix $\boldsymbol{A}_{\boldsymbol{\alpha\beta}}(\cdot)$ as follows:

$$
\begin{aligned}
\det(\boldsymbol{A}_{\boldsymbol{\alpha\beta}}(\cdot)) = \ & -\cos(\alpha)\cos(\theta)-\sin(\alpha)\sin(\theta)\cos(\phi)-\\
& \sin(\theta)\sin(\phi)\tan(\beta).
\end{aligned}
\tag{13.25}
$$

It can be seen from (13.25) that the matrix $\boldsymbol{A}_{\boldsymbol{\alpha\beta}}(\cdot)$ is not globally invertible even when $\phi = 0$ and $\theta \neq \pm 0.5\pi$. It is also observed that if we choose the angles α and β as the orientation coordinates for control design, there are a number of discontinuous surfaces, see (13.19), (13.20), and (13.21), which make the stability analysis difficult.

Using Angle γ. In this case, the path-following orientation error is defined as follows, see Figure 13.1:

$$
\gamma = e_\gamma - 2\pi n_\gamma(e_\gamma),
\tag{13.26}
$$

where

$$e_\gamma = \begin{cases} 2\arctan\left(\dfrac{\sqrt{a_2^2+a_3^2}}{a_1}\right); \left(a_1, \sqrt{a_2^2+a_3^2}\right) \neq (0,0), \\ 0; \left(a_1, \sqrt{a_2^2+a_3^2}\right) = (0,0). \end{cases} \tag{13.27}$$

The interpretation of the above expressions is similar to that of (13.18) and (13.19). It can be seen from (13.27) that e_γ is discontinuous on the following surface:

$$D_\gamma = \left\{ (a_1, a_2, a_3) : \sqrt{a_2^2+a_3^2} \neq 0, a_1 = 0 \right\}. \tag{13.28}$$

It can also be seen from (13.26) that γ is discontinuous on the surface:

$$C_\gamma = \{(a_1, a_2, a_3) : \gamma = \pi\}. \tag{13.29}$$

Differentiating both sides of (13.26) results in

$$\begin{aligned} \dot{\gamma} = \; & \frac{1}{e^2\sqrt{a_2^2+a_3^2}} \left(a_1 a_2 \left(\frac{\partial a_2}{\partial x_e}\dot{x}_e + \frac{\partial a_2}{\partial y_e}\dot{y}_e + \frac{\partial a_2}{\partial z_e}\dot{z}_e \frac{\partial a_2}{\partial \phi}\dot{\phi} \right) + \right. \\ & a_1 a_3 \left(\frac{\partial a_3}{\partial x_e}\dot{x}_e + \frac{\partial a_3}{\partial y_e}\dot{y}_e + \frac{\partial a_3}{\partial z_e}\dot{z}_e \frac{\partial a_3}{\partial \phi}\dot{\phi} \right) - \\ & \left(a_2^2+a_3^2\right) \left(\frac{\partial a_1}{\partial x_e}\dot{x}_e + \frac{\partial a_1}{\partial y_e}\dot{y}_e + \frac{\partial a_1}{\partial z_e}\dot{z}_e + \frac{\partial a_1}{\partial \phi}\dot{\phi} \right) + \\ & \left(a_1 \left(a_2 \frac{\partial a_2}{\partial \theta} + a_3 \frac{\partial a_3}{\partial \theta} \right) - \left(a_2^2+a_3^2\right) \frac{\partial a_1}{\partial \theta} \right) \dot{\theta} + \\ & \left. \left(a_1 \left(a_2 \frac{\partial a_2}{\partial \psi} + a_3 \frac{\partial a_3}{\partial \psi} \right) - \left(a_2^2+a_3^2\right) \frac{\partial a_1}{\partial \psi} \right) \dot{\psi} \right). \end{aligned} \tag{13.30}$$

Since

$$\begin{aligned} & \left[\frac{\left(a_1 \left(a_2 \dfrac{\partial a_2}{\partial \theta} + a_3 \dfrac{\partial a_3}{\partial \theta} \right) - \left(a_2^2+a_3^2\right) \dfrac{\partial a_1}{\partial \theta} \right)}{d_e^2 \sqrt{a_2^2+a_3^2}} \right]^2 + \\ & \left[\frac{\left(a_1 \left(a_2 \dfrac{\partial a_2}{\partial \psi} + a_3 \dfrac{\partial a_3}{\partial \psi} \right) - \left(a_2^2+a_3^2\right) \dfrac{\partial a_1}{\partial} \right)}{d_e^2 \sqrt{a_2^2+a_3^2}} \right]^2 \neq 0, \end{aligned} \tag{13.31}$$

for all $(x_e, y_e, z_e, \phi, \psi) \in \mathbb{R}^5$ and $\theta \in \mathbb{R} \backslash \pm 0.5\pi$, the angle γ can be chosen as the orientation coordinate for the control design. However (13.30) will result in a very

complicated control law.

Using a_1/d_e. By defining

$$\begin{aligned} a_e &= \sqrt{x_e^2 + y_e^2}, \\ \cos(\gamma_1) &= \frac{a_e}{d_e}\cos(\theta) - \frac{z_e}{d_e}\sin(\theta), \\ \cos(\gamma_2) &= \frac{x_e}{a_e}\cos(\psi) + \frac{y_e}{a_e}\sin(\psi), \end{aligned} \tag{13.32}$$

we can write a_1/d_e as follows

$$\frac{a_1}{d_e} = \cos(\gamma_1) + \frac{a_e}{d_e}\cos(\theta)(\cos(\gamma_2) - 1). \tag{13.33}$$

Since $\left|\frac{a_e}{d_e}\cos(\theta)\right| \leq 1$, $\forall\, (x_e, y_e, z_e, \theta) \in \mathbb{R}^4$, the conditions

$$\begin{aligned} \lim_{t\to\infty} \gamma_1 &= 0, \\ \lim_{t\to\infty} \gamma_2 &= 0 \end{aligned} \tag{13.34}$$

imply that $\lim_{t\to\infty}(a_1/d_e) = 1$. Furthermore, from (13.32) we can write

$$\begin{aligned} \gamma_1 &= \theta + \theta_d, \\ \gamma_2 &= \psi - \psi_d, \end{aligned} \tag{13.35}$$

where $\theta_d = \arccos(a_e/d_e)$ and $\psi_d = \arccos(x_e/a_e)$ are the desired orientation angles of the vessel in the horizontal and vertical planes, respectively. Hence (13.34) also implies the orientation control objective. If one differentiates both sides of (13.35) to obtain $\dot{\gamma}_1$ and $\dot{\gamma}_2$, there will be discontinuity in the γ_1- and γ_2- dynamics at $z_e = 0$ and/or $y_e = 0$, i.e., on the a_e and/or x_e axes. This discontinuity will cause difficulties in applying the backstepping technique. To get around this problem, we compute $\dot{\gamma}_1$ and $\dot{\gamma}_2$ based on (13.32) as follows:

$$\begin{aligned} \dot{\gamma}_1 &= \dot{\theta} + \frac{\dot{a}_e\sin(\theta) + \dot{z}_e\cos(\theta)}{d_e\cos(\gamma_1)} - \frac{\dot{d}_e\sin(\gamma_1)}{d_e\cos(\gamma_1)}, \\ \dot{\gamma}_2 &= \dot{\psi} + \frac{\dot{x}_e\sin(\psi) - \dot{y}_e\cos(\psi)}{a_e\cos(\gamma_2)} - \frac{\dot{a}_e\sin(\gamma_2)}{a_e\cos(\gamma_2)}. \end{aligned} \tag{13.36}$$

It can be seen that (13.36) is not defined at $\gamma_i = \pm 0.5\pi$, $i = 1, 2$, and $a_e = 0$, $d_e = 0$. However, our controller will guarantee that $|\gamma_i(t)| < 0.5\pi$ and $d_e(t) \geq d_e^*$, $a_e(t) \geq a_e^*$, $\forall\, t \geq t_0 \geq 0$ with arbitrarily small positive constants d_e^* and a_e^* and for feasible initial conditions. From (13.36), we can see that $\dot{\theta}$ and $\dot{\psi}$ are decoupled. Hence, designing a controller to achieve the control objective posed in the previous section by using the orientation coordinate a_1/d_e would be much simpler than using the angles γ, α, and β. For convenience of control design, we rewrite the transformed

system dynamics (13.15) and (13.36) as follows:

$$
\begin{aligned}
&\dot{d}_e = \frac{1}{d_e}\left(x_e\frac{\partial x_d}{\partial s} + y_e\frac{\partial y_d}{\partial s} + z_e\frac{\partial z_d}{\partial s}\right)\dot{s} - \frac{a_1}{d_e}u - \frac{a_2}{d_e}v - \frac{a_3}{d_e}w,\\
&\dot{\boldsymbol{\eta}}_{\boldsymbol{2\gamma}} = \boldsymbol{f}_{\boldsymbol{2\gamma}}(\cdot) + \boldsymbol{J}_{\boldsymbol{2}}(\boldsymbol{\eta}_{\boldsymbol{2}})\boldsymbol{v}_{\boldsymbol{2}},\\
&\boldsymbol{M}_{\boldsymbol{1}}\dot{\boldsymbol{v}}_{\boldsymbol{1}} = -\boldsymbol{C}_{\boldsymbol{1}}(\boldsymbol{v}_{\boldsymbol{1}})\boldsymbol{v}_{\boldsymbol{2}} - \boldsymbol{D}_{\boldsymbol{1}}(\boldsymbol{v}_{\boldsymbol{1}})\boldsymbol{v}_{\boldsymbol{1}} + \boldsymbol{\tau}_{\boldsymbol{1}} + \boldsymbol{\tau}_{\boldsymbol{1E}}(t),\\
&\boldsymbol{M}_{\boldsymbol{2}}\dot{\boldsymbol{v}}_{\boldsymbol{2}} = -\boldsymbol{C}_{\boldsymbol{1}}(\boldsymbol{v}_{\boldsymbol{1}})\boldsymbol{v}_{\boldsymbol{1}} - \boldsymbol{C}_{\boldsymbol{2}}(\boldsymbol{v}_{\boldsymbol{2}})\boldsymbol{v}_{\boldsymbol{2}} - \boldsymbol{D}_{\boldsymbol{2}}(\boldsymbol{v}_{\boldsymbol{2}})\boldsymbol{v}_{\boldsymbol{2}} - \boldsymbol{g}_{\boldsymbol{2}}(\boldsymbol{\eta}_{\boldsymbol{2}}) + \boldsymbol{\tau}_{\boldsymbol{2}} + \boldsymbol{\tau}_{\boldsymbol{2E}}(t),
\end{aligned}
\tag{13.37}
$$

where

$$
\begin{aligned}
&\boldsymbol{\eta}_{\boldsymbol{2\gamma}} = [\phi\ \gamma_1\ \gamma_2]^T,\\
&\boldsymbol{f}_{\boldsymbol{2\gamma}}(\cdot) = \begin{bmatrix} 0 \\ f_1^s\dot{s} + f_1^u u + f_1^v v + f_1^w w \\ f_2^s\dot{s} + f_2^u u + f_2^v v + f_2^w w \end{bmatrix},\\
&f_1^s = \varpi_{11}\frac{\partial x_d}{\partial s} + \varpi_{12}\frac{\partial y_d}{\partial s} + \varpi_{13}\frac{\partial z_d}{\partial s},\\
&f_1^u = -\left[\varpi_{11}J_1^{11}(\boldsymbol{\eta}_{\boldsymbol{2}}) + \varpi_{12}J_1^{21}(\boldsymbol{\eta}_{\boldsymbol{2}}) + \varpi_{13}J_1^{31}(\boldsymbol{\eta}_{\boldsymbol{2}})\right],\\
&f_1^v = -\left[\varpi_{11}J_1^{12}(\boldsymbol{\eta}_{\boldsymbol{2}}) + \varpi_{12}J_1^{22}(\boldsymbol{\eta}_{\boldsymbol{2}}) + \varpi_{13}J_1^{32}(\boldsymbol{\eta}_{\boldsymbol{2}})\right],\\
&f_1^w = -\left[\varpi_{11}J_1^{13}(\boldsymbol{\eta}_{\boldsymbol{2}}) + \varpi_{12}J_1^{23}(\boldsymbol{\eta}_{\boldsymbol{2}}) + \varpi_{13}J_1^{33}(\boldsymbol{\eta}_{\boldsymbol{2}})\right],\\
&f_2^s = \varpi_{21}\frac{\partial x_d}{\partial s} + \varpi_{22}\frac{\partial y_d}{\partial s},\\
&f_2^u = -\left[\varpi_{21}J_1^{11}(\boldsymbol{\eta}_{\boldsymbol{2}}) + \varpi_{22}J_1^{21}(\boldsymbol{\eta}_{\boldsymbol{2}})\right],\\
&f_2^v = -\left[\varpi_{21}J_1^{12}(\boldsymbol{\eta}_{\boldsymbol{2}}) + \varpi_{22}J_1^{22}(\boldsymbol{\eta}_{\boldsymbol{2}})\right],\\
&f_2^w = -\left[\varpi_{21}J_1^{13}(\boldsymbol{\eta}_{\boldsymbol{2}}) + \varpi_{22}J_1^{23}(\boldsymbol{\eta}_{\boldsymbol{2}})\right],
\end{aligned}
\tag{13.38}
$$

with

$$
\begin{aligned}
\varpi_{11} &= \left(\frac{x_e\sin(\theta)}{a_e d_e\cos(\gamma_1)} - \frac{x_e\sin(\gamma_1)}{d_e^2\cos(\gamma_1)}\right),\\
\varpi_{12} &= \left(\frac{y_e\sin(\theta)}{a_e d_e\cos(\gamma_1)} - \frac{y_e\sin(\gamma_1)}{d_e^2\cos(\gamma_1)}\right),\\
\varpi_{13} &= \left(\frac{\cos(\theta)}{d_e\cos(\gamma_1)} - \frac{z_e\sin(\gamma_1)}{d_e^2\cos(\gamma_1)}\right),\\
\varpi_{21} &= \left(\frac{\sin(\psi)}{a_e\cos(\gamma_2)} - \frac{x_e\sin(\gamma_2)}{a_e^2\cos(\gamma_2)}\right),\\
\varpi_{22} &= \left(-\frac{\cos(\psi)}{a_e\cos(\gamma_2)} - \frac{y_e\sin(\gamma_2)}{a_e^2\cos(\gamma_2)}\right).
\end{aligned}
\tag{13.39}
$$

Therefore, we will design the control inputs $\boldsymbol{\tau}_{\boldsymbol{1}}$ and $\boldsymbol{\tau}_{\boldsymbol{2}}$ for (13.37) to yield the control objective. In Section 13.3, a procedure to design a stabilizer for the path-

following error system (13.37) is presented in detail. The structure of (13.37) suggests that we design the actual controls $\boldsymbol{\tau_1}$ and $\boldsymbol{\tau_2}$ in two stages. First, we design the virtual velocity controls for u and $\boldsymbol{v}_2$ and choose $\dot{s}$ to ultimately stabilize d_e and $\gamma_i, i = 1,2$ at the origin. Based on the backstepping technique, the controls $\boldsymbol{\tau_1}$ and $\boldsymbol{\tau_2}$ will then be designed to make the errors between the virtual velocity controls and their actual values asymptotically tend to a small ball centered at the origin. Since the vessel parameters are unknown, an adaptation scheme is also introduced in this step to estimate their values used in the control laws. We split the control design procedure into two steps. The first step is to design $\boldsymbol{\tau_1}$ while the second step takes care of $\boldsymbol{\tau_2}$. This allows us to simplify the choice of feasible initial conditions.

Since the transformed system (13.37) is not defined at $d_e(t) = 0$, $a_e(t) = 0$, $\gamma_i(t) = \pm 0.5\pi, i = 1,2$, we first assume that

$$d_e(t) \geq d_e^*, a_e(t) \geq a_e^*, |\gamma_i(t)| < 0.5\pi,\ i = 1,2,\ \forall t \geq t_0 \geq 0, \tag{13.40}$$

for some positive constants d_e^* and a_e^*. Our controller design will guarantee (13.40) for feasible initial conditions.

13.3 Control Design

The d_e-dynamics have two inputs that can be chosen to stabilize d_e, namely $\dot{s}$ and u. We can either choose the input u or $\dot{s}$ and then design the remaining input. If we fix $\dot{s}$, then the virtual vessel is allowed to move at a desired speed. The real vessel will follow the virtual one on the path by the controller, and vice versa. In this chapter, we choose to fix $\dot{s}$. This allows us to adjust the initial conditions in most cases without moving the real vessel, see Section 13.4.

Define

$$\tilde{u} = u - u_d, \tag{13.41}$$

where u_d is the intermediate control of u. As discussed above, we choose the intermediate control u_d and $\dot{s}$ as follows:

$$u_d = k_1(d_e - \delta_e) - \frac{1}{a_1}(a_2 v + a_3 w) + \frac{1}{d_e}\frac{u_0(t,d_e)\left(x_e\frac{\partial x_d}{\partial s} + y_e\frac{\partial y_d}{\partial s} + z_e\frac{\partial z_d}{\partial s}\right)}{\sqrt{\left(\frac{\partial x_d}{\partial s}\right)^2 + \left(\frac{\partial y_d}{\partial s}\right)^2 + \left(\frac{\partial z_d}{\partial s}\right)^2}}, \tag{13.42}$$

$$\dot{s} = \frac{a_1}{d_e}\frac{u_0(t,d_e)}{\sqrt{\left(\frac{\partial x_d}{\partial s}\right)^2 + \left(\frac{\partial y_d}{\partial s}\right)^2 + \left(\frac{\partial z_d}{\partial s}\right)^2}}, \tag{13.43}$$

where k_1 and δ_e are positive constants to be selected later, and $u_0(t,d_e) \neq 0$, $\forall t \geq t_0 \geq 0$, $d_e(t) \in \mathbb{R}$, is the speed of the virtual vessel on the path. Indeed, one can

choose this speed to be a constant. However, the time-varying speed and position path-following error dependence of the virtual vessel on the path is more desirable, especially when the underwater vehicle starts to follow the path. For example, one might choose

$$u_0(t,d_e) = u_0^*(1-\chi_1 e^{-\chi_2(t-t_0)})e^{-\chi_3 d_e}, \tag{13.44}$$

where $u_0^* \neq 0$, $\chi_i > 0, i = 1,2,3$, $\chi_1 < 1$. The choice of $u_0(t,d_e)$ in (13.44) has the following desired feature: When the path-following error, d_e, is large, the virtual vessel will wait for the real one; when d_e is small the virtual vessel will move along the path at the speed closed to u_0^* and the real one follows it within the specified look ahead distance. This feature is suitable in practice because it avoids using a high-gain control for large signal d_e. It is noted that u_d is not defined at $a_1 = 0$. Since the terms a_2/a_1 and a_3/a_1 can be written as $(a_2/d_e)/(a_1/d_e)$ and $(a_3/d_e)/(a_1/d_e)$, and recalling that $\cos(\gamma) = a_1/d_e$, the intermediate control u_d is well defined if (13.40) holds and

$$|\gamma(t)| < 0.5\pi, \forall t \geq t_0 \geq 0. \tag{13.45}$$

We will come back to this issue in Section 13.4.

Remark 13.2.

1. If we design the virtual control u_d without canceling the terms $a_2 v$ and $a_3 w$ in the d_e-dynamics, then the condition (13.45) is not required for u_d being well defined. However, an assumption of the sway and heave velocities being bounded is needed in advance in the stability analysis, i.e. assume stability to prove stability.
2. If the sway and heave velocities are assumed to be bounded by the surge velocity, the terms $a_2 v$ and $a_3 w$ are not required to be canceled either. This controller can be designed similarly to the one in this chapter. It is noted that the sway velocity does not require to be bounded by the surge velocity with a relatively small constant as in [129] for the case of path-following in the horizontal plane.

Substituting (13.42) and (13.43) into the first equation of (13.37) results in

$$\dot{d}_e = -k_1 \frac{a_1}{d_e}(d_e - \delta_e) - \frac{a_1}{d_e}\tilde{u}. \tag{13.46}$$

By noticing that under Assumption 13.1, see (13.40) and (13.45), the intermediate control u_d is a smooth function of $x_e, y_e, z_e, s, u_0, \eta_2, v$, and w, differentiating both sides of (13.41) with (13.42) and (13.43) yields

$$\begin{aligned}\dot{\tilde{u}} = {} & \frac{m_{22}}{m_{11}} vr - \frac{m_{33}}{m_{11}} wq - \frac{d_{11}}{m_{11}} u - \sum_{i=2}^{3} \frac{d_{ui}}{m_{11}} |u|^{i-1} u + \frac{1}{m_{11}} \tau_u + \\ & \frac{1}{m_{11}} \tau_{wu}(t) - \frac{\partial u_d}{\partial x_e} \dot{x}_e - \frac{\partial u_d}{\partial y_e} \dot{y}_e - \frac{\partial u_d}{\partial z_e} \dot{z}_e - \frac{\partial u_d}{\partial s} \dot{s} - \frac{\partial u_d}{\partial u_0} \dot{u}_0 - \\ & \frac{\partial u_d}{\partial \boldsymbol{\eta_2}} \dot{\boldsymbol{\eta}}_{\mathbf{2}} - \frac{\partial u_d}{\partial v} \left(\frac{m_{33}}{m_{22}} wp - \frac{m_{11}}{m_{22}} ur - \frac{d_{22}}{m_{22}} v - \sum_{i=2}^{3} \frac{d_{vi}}{m_{22}} |v|^{i-1} v + \right.\end{aligned}$$

$$\frac{1}{m_{22}}\tau_{wv}(t)\Big) - \frac{\partial u_d}{\partial w}\left(\frac{m_{11}}{m_{33}}uq - \frac{m_{22}}{m_{33}}vp - \frac{d_{33}}{m_{33}}w - \sum_{i=2}^{3}\frac{d_{wi}}{m_{33}}|w|^{i-1}w + \frac{1}{m_{33}}\tau_{ww}(t)\right), \tag{13.47}$$

where for convenience of choosing u_0, the terms $\frac{\partial u_d}{\partial x_e}$, $\frac{\partial u_d}{\partial y_e}$, and $\frac{\partial u_d}{\partial z_e}$ do not include $\frac{\partial u_0}{\partial x_e}$, $\frac{\partial u_0}{\partial y_e}$ and $\frac{\partial u_0}{\partial z_e}$, which are lumped into $\dot{u}_0$. From (13.47), we choose the actual control $\boldsymbol{\tau_1}$ or τ_u without canceling useful nonlinear damping terms as

$$\begin{aligned}\tau_u = \; & -c_1\tilde{u} - \hat{\theta}_1^T f_1(\cdot) - \hat{\theta}_{21}\tanh\left(\frac{\tilde{u}\hat{\theta}_{21}}{\varepsilon_{21}}\right) - \hat{\theta}_{22}\frac{\partial u_d}{\partial v}\tanh\left(\frac{\partial u_d}{\partial v}\frac{\tilde{u}\hat{\theta}_{22}}{\varepsilon_{22}}\right) - \\ & \hat{\theta}_{23}\frac{\partial u_d}{\partial w}\tanh\left(\frac{\partial u_d}{\partial w}\frac{\tilde{u}\hat{\theta}_{23}}{\varepsilon_{23}}\right),\end{aligned} \tag{13.48}$$

and the update law as

$$\begin{aligned}\dot{\hat{\theta}}_{1j} &= \gamma_{1j}\text{proj}\left(\tilde{u}\, f_{1j}(\cdot), \hat{\theta}_{1j}\right),\ 1 \le j \le 16, \\ \dot{\hat{\theta}}_{21} &= \gamma_{21}\text{proj}\left(|\tilde{u}|, \hat{\theta}_{21}\right), \\ \dot{\hat{\theta}}_{22} &= \gamma_{22}\text{proj}\left(\left|\tilde{u}\frac{\partial u_d}{\partial v}\right|, \hat{\theta}_{22}\right), \\ \dot{\hat{\theta}}_{23} &= \gamma_{23}\text{proj}\left(\left|\tilde{u}\frac{\partial u_d}{\partial w}\right|, \hat{\theta}_{23}\right),\end{aligned} \tag{13.49}$$

where $c_1, \varepsilon_{2i}, \gamma_{1j}, \gamma_{2i}, 1 \le i \le 3$ and $1 \le j \le 16$, are positive constants to be selected later, and $f_{1j}(\cdot)$ are the jth elements of $f_1(\cdot)$, respectively, with

$$\begin{aligned}f_1(\cdot) = \Bigg[& vr, -wq, -u_d, -|u|u_d, -u^2u_d, -\left(\frac{\partial u_d}{\partial x_e}\dot{x}_e + \frac{\partial u_d}{\partial y_e}\dot{y}_e + \frac{\partial u_d}{\partial z_e}\dot{z}_e + \right. \\ & \left.\frac{\partial u_d}{\partial s}\dot{s} + \frac{\partial u_d}{\partial u_0}\dot{u}_0 + \frac{\partial u_d}{\partial \boldsymbol{\eta_2}}\dot{\boldsymbol{\eta}}_{\boldsymbol{2}}\right), -\frac{\partial u_d}{\partial v}wp, \frac{\partial u_d}{\partial v}ur, \frac{\partial u_d}{\partial v}v, \frac{\partial u_d}{\partial v}|v|v, \\ & \frac{\partial u_d}{\partial v}v^3, -\frac{\partial u_d}{\partial w}uq, \frac{\partial u_d}{\partial w}vp, \frac{\partial u_d}{\partial w}w, \frac{\partial u_d}{\partial w}|w|w, \frac{\partial u_d}{\partial w}w^3\Bigg]^T,\end{aligned} \tag{13.50}$$

$\hat{\theta}_{ij},\ 1 \le i \le 2$ is the jth element of $\hat{\theta}_i$, which is an estimate of θ_i with

$$\begin{aligned}\theta_1 = \Bigg[& m_{22}, m_{33}, d_{11}, d_{u2}, d_{u3}, m_{11}, \frac{m_{11}m_{33}}{m_{22}}, \frac{m_{11}^2}{m_{22}}, \frac{m_{11}d_{22}}{m_{22}}, \frac{m_{11}d_{v2}}{m_{22}}, \\ & \frac{m_{11}d_{v3}}{m_{22}}, \frac{m_{11}^2}{m_{33}}, \frac{m_{11}m_{22}}{m_{33}}, \frac{m_{11}d_{33}}{m_{33}}, \frac{m_{11}d_{w2}}{m_{33}}, \frac{m_{11}d_{w3}}{m_{33}}\Bigg]^T,\end{aligned}$$

$$\theta_2 = \left[\tau_{wu}^{\max}, \frac{m_{11}}{m_{22}}\tau_{wv}^{\max}, \frac{m_{11}}{m_{33}}\tau_{ww}^{\max}\right]^T. \tag{13.51}$$

The operator, proj, is the Lipschitz continuous projection algorithm repeated here for the convenience of the reader as follows:

$$\begin{aligned}
&\text{proj}(\varpi, \hat{\omega}) = \varpi \qquad \text{if} \quad \Xi(\hat{\omega}) \le 0,\\
&\text{proj}(\varpi, \hat{\omega}) = \varpi \qquad \text{if} \quad \Xi(\hat{\omega}) \ge 0 \text{ and } \Xi_{\hat{\omega}}(\hat{\omega})\varpi \le 0,\\
&\text{proj}(\varpi, \hat{\omega}) = (1 - \Xi(\hat{\omega}))\varpi \quad \text{if } \Xi(\hat{\omega}) > 0 \text{ and } \Xi_{\hat{\omega}}(\hat{\omega})\varpi > 0,
\end{aligned} \tag{13.52}$$

where $\Xi(\hat{\omega}) = \frac{\hat{\omega}^2 - \omega_M^2}{\mu^2 + 2\mu\omega_M}$, $\Xi_{\hat{\omega}}(\hat{\omega}) = \frac{\partial \Xi(\hat{\omega})}{\partial \hat{\omega}}$, μ is an arbitrarily small positive constant, $\hat{\omega}$ is an estimate of ω and $|\omega| \le \omega_M$.

The projection algorithm is such that if $\dot{\hat{\omega}} = \text{proj}(\varpi, \hat{\omega})$ and $\hat{\omega}(t_0) \le \omega_M$ and then

1. $\hat{\omega}(t) \le \omega_M + \xi$, $\forall\, 0 \le t_0 \le t < \infty$,
2. proj$(\varpi, \hat{\omega})$ is Lipschitz continuous,
3. $|\text{proj}(\varpi, \hat{\omega})| \le |\varpi|$,
4. $\tilde{\omega}\text{proj}(\varpi, \hat{\omega}) \ge \tilde{\omega}\varpi$ with $\tilde{\omega} = \omega - \hat{\omega}$.

Substituting (13.48) into (13.47) yields the error dynamics

$$\begin{aligned}
\dot{\tilde{u}} \;=& -\frac{1}{m_{11}}\left(c_1 + d_{11} + \sum_{i=2}^{3} d_{ui}\,|u|^{i-1}\right)\tilde{u} + \frac{1}{m_{11}}\theta_1^T f_1(\cdot) - \frac{1}{m_{11}}\hat{\theta}_1^T f_1(\cdot) + \\
&\frac{1}{m_{11}}\tau_{wu}(t) - \frac{1}{m_{11}}\hat{\theta}_{21}\tanh\left(\frac{\tilde{u}\hat{\theta}_{21}}{\varepsilon_{21}}\right) - \frac{\partial u_d}{\partial v}\frac{1}{m_{22}}\tau_{wv}(t) - \frac{1}{m_{11}}\hat{\theta}_{22}\frac{\partial u_d}{\partial v}\times \\
&\tanh\left(\frac{\partial u_d}{\partial v}\frac{\tilde{u}\hat{\theta}_{22}}{\varepsilon_{22}}\right) - \frac{\partial u_d}{\partial w}\frac{1}{m_{33}}\tau_{ww}(t) - \frac{1}{m_{11}}\hat{\theta}_{23}\frac{\partial u_d}{\partial w}\tanh\left(\frac{\partial u_d}{\partial w}\frac{\tilde{u}\hat{\theta}_{23}}{\varepsilon_{23}}\right).
\end{aligned} \tag{13.53}$$

Define

$$\tilde{\boldsymbol{v}}_{\boldsymbol{2}} = \boldsymbol{v}_{\boldsymbol{2}} - \boldsymbol{v}_{\boldsymbol{2d}}, \tag{13.54}$$

where $\boldsymbol{v}_{\boldsymbol{2d}} = [p_d, q_d, r_d]^T$ is the intermediate control of $\boldsymbol{v}_{\boldsymbol{2}}$. Recalling that our goal is to ultimately stabilize $\boldsymbol{\eta}_{\boldsymbol{2\gamma}} = [\phi, \gamma_1, \gamma_2]^T$ at the origin, the second equation of (13.37) suggests that we choose this intermediate control as follows:

$$\boldsymbol{v}_{\boldsymbol{2d}} = \boldsymbol{J}_{\boldsymbol{2}}^{-\boldsymbol{1}}(\boldsymbol{\eta}_{\boldsymbol{2}})\left(-\boldsymbol{f}_{\boldsymbol{2\gamma}}(\cdot) - \boldsymbol{K}_{\boldsymbol{2}}\boldsymbol{\eta}_{\boldsymbol{2\gamma}}\right), \tag{13.55}$$

where $\boldsymbol{K}_{\boldsymbol{2}} = \text{diag}(k_{21}, k_{22}, k_{23})$ is a positive definite diagonal matrix. Substituting (13.54) and (13.55) into the second equation of (13.37) yields

$$\dot{\boldsymbol{\eta}}_{\boldsymbol{2\gamma}} = -\boldsymbol{K}_{\boldsymbol{2}}\boldsymbol{\eta}_{\boldsymbol{2\gamma}} + \boldsymbol{J}_{\boldsymbol{2}}(\boldsymbol{\eta}_{\boldsymbol{2}})\tilde{\boldsymbol{v}}_{\boldsymbol{2}}. \tag{13.56}$$

To design the actual control $\boldsymbol{\tau_2}$, we first note that under Assumption 13.1, (13.40) and (13.45), the intermediate control $\boldsymbol{v_{2d}}$ is a smooth function of $x_e, y_e, z_e, s, u_0, \boldsymbol{\eta_2}$, and $\boldsymbol{v_1}$. Differentiating both sides of (13.54) and multiplying by $\boldsymbol{M_2}$, along the solutions of the last two equations of (13.37) results in

$$\boldsymbol{M_2}\dot{\tilde{\boldsymbol{v}}}_{\boldsymbol{2}} = -\boldsymbol{C_2}(\boldsymbol{v_2})\tilde{\boldsymbol{v}}_{\boldsymbol{2}} - \boldsymbol{D_2}(\boldsymbol{v_2})\tilde{\boldsymbol{v}}_{\boldsymbol{2}} + \boldsymbol{F}(\cdot)\boldsymbol{\theta_3} + \boldsymbol{G}(\cdot)\boldsymbol{\theta_4}(t) + \boldsymbol{\tau_2}, \tag{13.57}$$

where

$$\begin{aligned}
\boldsymbol{F}(\cdot)\boldsymbol{\theta_3} = &-\boldsymbol{C_1}(\boldsymbol{v_1})\boldsymbol{v_1} - \boldsymbol{C_2}(\boldsymbol{v_2})\boldsymbol{v_{2d}} - \boldsymbol{D_2}(\boldsymbol{v_2})\boldsymbol{v_{2d}} - \boldsymbol{g_2}(\boldsymbol{\eta_2}) - \\
&\boldsymbol{M_2}\left(\frac{\partial \boldsymbol{v_{2d}}}{\partial x_e}\dot{x}_e + \frac{\partial v_{2d}}{\partial y_e}\dot{y}_e + \frac{\partial \boldsymbol{v_{2d}}}{\partial z_e}\dot{z}_e + \frac{\partial \boldsymbol{v_{2d}}}{\partial s}\dot{s} + \frac{\partial \boldsymbol{v_{2d}}}{\partial u_0}\dot{u}_0 + \right. \\
&\left.\frac{\partial \boldsymbol{v_{2d}}}{\partial \boldsymbol{\eta_2}}\dot{\boldsymbol{\eta}}_{\boldsymbol{2}}\right) - \boldsymbol{M_2}\frac{\partial \boldsymbol{v_{2d}}}{\partial \boldsymbol{v_1}}\boldsymbol{M_1^{-1}}(-\boldsymbol{C_1}(\boldsymbol{v_1})\boldsymbol{v_2} - \boldsymbol{D_1}(\boldsymbol{v_1})\boldsymbol{v_1} + \boldsymbol{\tau_1}), \\
\boldsymbol{G}(\cdot)\boldsymbol{\theta_4}(t) = &\boldsymbol{\tau_{w2}}(t) - \boldsymbol{M_2}\frac{\partial \boldsymbol{v_{2d}}}{\partial \boldsymbol{v_1}}\boldsymbol{M_1^{-1}}\boldsymbol{\tau_{w1}}(t),
\end{aligned} \tag{13.58}$$

with $\boldsymbol{F}(\cdot) \in \mathbb{R}^{3\times m_3}$ and $\boldsymbol{G}(\cdot) \in \mathbb{R}^{3\times m_4}$ being the regression matrices, $\boldsymbol{\theta_3} \in \mathbb{R}^{3\times m_3}$ and $\boldsymbol{\theta_4}(t) \in \mathbb{R}^{m_4}$ being the vectors of unknown vessel and environmental disturbance parameters. For the sake of simplicity, the regression matrices $\boldsymbol{F}(\cdot)$ and $\boldsymbol{G}(\cdot)$, and the vectors $\boldsymbol{\theta_3}$ and $\boldsymbol{\theta_4}(t)$ are not written down explicitly. From (13.56) and (13.57), we choose the actual control $\boldsymbol{\tau_2}$ and update laws as follows:

$$\boldsymbol{\tau_2} = -\boldsymbol{K_3}\tilde{\boldsymbol{v}}_{\boldsymbol{2}} - \left(\boldsymbol{\eta_{2\gamma}^T}\boldsymbol{J_2}(\boldsymbol{\eta_2})\right)^{\boldsymbol{T}} - \boldsymbol{F}(\cdot)\hat{\boldsymbol{\theta}}_{\boldsymbol{3}} - \boldsymbol{G}(\cdot)\hat{\boldsymbol{\theta}}_{\boldsymbol{4}}, \tag{13.59}$$

$$\begin{aligned}
\dot{\hat{\theta}}_{3i} &= \gamma_{3i}\mathrm{proj}\left(\sum_{j=1}^{3}\tilde{v}_{2j}f_{ji}, \hat{\theta}_{3i}\right), 1 \le i \le m_3, \\
\dot{\hat{\theta}}_{4i} &= \gamma_{4i}\mathrm{proj}\left(\sum_{j=1}^{3}\left|\tilde{v}_{2j}g_{ji}\right|, \hat{\theta}_{4i}\right), 1 \le i \le m_4,
\end{aligned} \tag{13.60}$$

where $\varepsilon_{4i} > 0,\ 1 \le i \le 3, \gamma_{3j} > 0,\ 1 \le j \le m_3, \gamma_{4l} > 0,\ 1 \le l \le m_4$, $\boldsymbol{K_3} = \mathrm{diag}(k_{31}, k_{32}, k_{33})$ is a positive definite diagonal matrix,$\hat{\theta}_{3i}$ is an estimate of the ith element of $\boldsymbol{\theta_3}$, and $\hat{\theta}_{4i}$ is an estimate of the maximum value of the ith element of $\boldsymbol{\theta_4}(t)$. For simplicity of notation, we have defined

$$\boldsymbol{F}(\cdot)\hat{\boldsymbol{\theta}}_{\boldsymbol{3}} := \begin{bmatrix} \sum_{i=1}^{m_3} f_{1i}\hat{\theta}_{3i} \\ \sum_{i=1}^{m_3} f_{2i}\hat{\theta}_{3i} \\ \sum_{i=1}^{m_3} f_{3i}\hat{\theta}_{3i} \end{bmatrix},\ \boldsymbol{G}(\cdot)\hat{\boldsymbol{\theta}}_{\boldsymbol{4}} := \begin{bmatrix} \sum_{i=1}^{m_4} g_{1i}\hat{\theta}_{4i}\tanh\left(\varepsilon_{41}^{-1}\tilde{v}_{21}\sum_{i=1}^{m_2} g_{1i}\hat{\theta}_{4i}\right) \\ \sum_{i=1}^{m_4} g_{2i}\hat{\theta}_{4i}\tanh\left(\varepsilon_{42}^{-1}\tilde{v}_{22}\sum_{i=1}^{m_2} g_{2i}\hat{\theta}_{4i}\right) \\ \sum_{i=1}^{m_4} g_{3i}\hat{\theta}_{4i}\tanh\left(\varepsilon_{43}^{-1}\tilde{v}_{23}\sum_{i=1}^{m_2} g_{3i}\hat{\theta}_{4i}\right) \end{bmatrix}, \tag{13.61}$$

with f_{ji}, $1 \leq j \leq 3$, $1 \leq i \leq m_3$, being the element in jth column and ith row of the regression matrix $\boldsymbol{F}(\cdot)$. Similarly g_{ji}, $1 \leq j \leq 3$, $1 \leq i \leq m_4$, is the element in jth column and ith row of the regression matrix $\boldsymbol{G}(\cdot)$.

Substituting (13.59) into (13.57) yields the error dynamics

$$\begin{aligned}\boldsymbol{M_2}\dot{\tilde{\boldsymbol{v}}}_{\boldsymbol{2}} = & -\boldsymbol{C_2}(\boldsymbol{v_2})\tilde{\boldsymbol{v}}_{\boldsymbol{2}} - (\boldsymbol{K_3} + \boldsymbol{D_2}(\boldsymbol{v_2}))\tilde{\boldsymbol{v}}_{\boldsymbol{2}} - \left(\boldsymbol{\eta}_{\boldsymbol{2\gamma}}^{\boldsymbol{T}}\boldsymbol{J_2}(\boldsymbol{\eta_2})\right)^{\boldsymbol{T}} + \boldsymbol{F}(\cdot)\boldsymbol{\theta_3} + \\ & \boldsymbol{G}(\cdot)\boldsymbol{\theta_4}(t) - \boldsymbol{F}(\cdot)\hat{\boldsymbol{\theta}}_{\boldsymbol{3}} - \boldsymbol{G}(\cdot)\hat{\boldsymbol{\theta}}_{\boldsymbol{4}}. \end{aligned} \tag{13.62}$$

We now present the main result of this chapter, the proof of which is given in the next section.

Theorem 13.1. *Assume that*

1. *the vessel inertia, added mass and damping matrices are diagonal;*
2. *the environmental disturbances are bounded;*
3. *the vessel parameters are unknown but constant;*
4. *the reference path satisfies Assumption 13.1.*

If the state feedback control laws (13.48) and (13.59), and the update laws (13.49) and (13.60) are applied to the vessel system (13.1) then there exist feasible initial conditions such that the path-following errors $(x(t) - x_d(t), y(t) - y_d(t), z(t) - z_d(t), \gamma_1(t), \gamma_2(t))$ *converge to a ball centered on the desired path* $\boldsymbol{\Omega}$ *asymptotically. Furthermore, the radius of this ball can be made arbitrarily small by adjusting the control gains.*

13.4 Stability Analysis

To prove Theorem 13.1, we first consider the $\left(\boldsymbol{\eta_{2\gamma}}, \tilde{\boldsymbol{v}}_{\boldsymbol{2}}\right)$-subsystem and then the $(\boldsymbol{d_e}, \tilde{\boldsymbol{u}})$-subsystem.

$\left(\boldsymbol{\eta_{2\gamma}}, \tilde{\boldsymbol{v}}_{\boldsymbol{2}}\right)$-subsystem

To investigate stability of this subsystem, we consider the following Lyapunov function

$$V_1 = \frac{1}{2}\boldsymbol{\eta}_{\boldsymbol{2\gamma}}^{\boldsymbol{T}}\boldsymbol{\eta_{2\gamma}} + \frac{1}{2}\tilde{\boldsymbol{v}}_{\boldsymbol{2}}^{\boldsymbol{T}}\boldsymbol{M_2}\tilde{\boldsymbol{v}}_{\boldsymbol{2}} + \frac{1}{2}\sum_{i=3}^{4}\tilde{\boldsymbol{\theta}}_{\boldsymbol{i}}^{\boldsymbol{T}}\boldsymbol{\Gamma_i^{-1}}\tilde{\boldsymbol{\theta}}_{\boldsymbol{i}}, \tag{13.63}$$

where $\tilde{\boldsymbol{\theta}}_{\boldsymbol{i}} = \boldsymbol{\theta_i} - \hat{\boldsymbol{\theta}}_{\boldsymbol{i}}$ and $\boldsymbol{\Gamma_i} = \mathrm{diag}\left(\gamma_{ij}\right)$, $1 \leq j \leq m_3$ for $i = 3$, $1 \leq j \leq m_4$ for $i = 4$. Differentiating both sides of (13.63) along (13.56), (13.60), and (13.62) yields

$$\dot{V}_1 \leq -\boldsymbol{\eta}_{\boldsymbol{2\gamma}}^{\boldsymbol{T}}\boldsymbol{K_2}\boldsymbol{\eta_{2\gamma}} - \tilde{\boldsymbol{v}}_{\boldsymbol{2}}^{\boldsymbol{T}}\left(\boldsymbol{D_{20}} + \boldsymbol{K_3}\right)\tilde{\boldsymbol{v}}_{\boldsymbol{2}} + 0.2785\sum_{i=1}^{3}\varepsilon_{4i}, \tag{13.64}$$

where $\boldsymbol{D_{20}} = \mathrm{diag}(d_{44}, d_{55}, d_{66})$ and we have used $|x| - x\tanh(x/\lambda) \leq 0.2785\lambda$ for all $x \in \mathbb{R}$ and $\lambda > 0$. From (13.64), we conclude that $\boldsymbol{\eta_{2\gamma}}$ and $\tilde{\boldsymbol{v}}_{\boldsymbol{2}}$ are ultimately asymptotically stable at the origin. To estimate the upper bound of $\boldsymbol{\eta_{2\gamma}}$ and $\tilde{\boldsymbol{v}}_{\boldsymbol{2}}$, we subtract and add $\frac{1}{2}\sum_{i=3}^{4} \tilde{\boldsymbol{\theta}}_{\boldsymbol{i}}^{\boldsymbol{T}} \boldsymbol{\Gamma}_{\boldsymbol{i}}^{-\mathbf{1}} \tilde{\boldsymbol{\theta}}_{\boldsymbol{i}}$ to the right-hand side of (13.64) to obtain

$$\dot{V}_1 \leq -\sigma_1 V_1 + \rho_1, \tag{13.65}$$

where

$$\begin{aligned} \sigma_1 &= \min\left(1, 2\lambda_{\min}(\boldsymbol{K_2}), \frac{2\lambda_{\min}(\boldsymbol{D_{20}} + \boldsymbol{K_3})}{\lambda_{\max}(\boldsymbol{M_2})}\right), \\ \rho_1 &= \frac{1}{2}\sum_{i=3}^{4} \tilde{\boldsymbol{\theta}}_{\boldsymbol{i}}^{\boldsymbol{T}} \boldsymbol{\Gamma}_{\boldsymbol{i}}^{-\mathbf{1}} \tilde{\boldsymbol{\theta}}_{\boldsymbol{i}} + 0.2785\sum_{i=1}^{3} \varepsilon_{4i}. \end{aligned} \tag{13.66}$$

From (13.65), it is direct to show that

$$V_1(t) \leq V_1(t_0) e^{-\sigma_1(t-t_0)} + \frac{\rho_1}{\sigma_1}, \tag{13.67}$$

which further yields

$$\begin{aligned} \left\|\boldsymbol{\eta_{2\gamma}}(\boldsymbol{t})\right\| &\leq \sqrt{2V_1(t_0)}\, e^{-\frac{\sigma_1}{2}(t-t_0)} + \sqrt{\frac{2\rho_1}{\sigma_1}} := \alpha_\eta(\cdot) e^{-\frac{\sigma_1}{2}(t-t_0)} + \rho_\eta, \\ \left\|\tilde{\boldsymbol{v}}_{\boldsymbol{2}}(\boldsymbol{t})\right\| &\leq \sqrt{\frac{2V_1(t_0)}{\lambda_{\min}(\boldsymbol{M_2})}}\, e^{-\frac{\sigma_1}{2}(t-t_0)} + \sqrt{\frac{2\rho_1}{\sigma_1\lambda_{\min}(\boldsymbol{M_2})}} := \alpha_v(\cdot) e^{-\frac{\sigma_1}{2}(t-t_0)} + \rho_v. \end{aligned} \tag{13.68}$$

$(d_e, \tilde{u})$-subsystem

To analyze the stability of this subsystem more easily, we first consider the $\tilde{u}$-dynamics and then the d_e-dynamics.

$\tilde{u}$-dynamics. Consider the following Lyapunov function

$$V_2 = \frac{m_{11}}{2}\tilde{u}^2 + \frac{1}{2}\sum_{i=1}^{2} \tilde{\theta}_i^T \Gamma_i^{-1} \tilde{\theta}_i, \tag{13.69}$$

where $\tilde{\theta}_i = \theta_i - \hat{\theta}_i$ and $\Gamma_i = \mathrm{diag}\left(\gamma_{ij}\right)$, $1 \leq j \leq 16$ for $i = 1$, $1 \leq j \leq 3$ for $i = 2$. Differentiating both sides of (13.69) along (13.47), (13.48), and (13.49) yields

$$\dot{V}_2 \leq -(c_1 + d_{11})\tilde{u}^2 + 0.2785\sum_{i=1}^{3} \varepsilon_{2i}. \tag{13.70}$$

Subtracting and adding $\frac{1}{2}\sum_{i=1}^{2}\tilde{\boldsymbol{\theta}}_{\boldsymbol{i}}^{\boldsymbol{T}}\boldsymbol{\Gamma}_{\boldsymbol{i}}^{-\mathbf{1}}\tilde{\boldsymbol{\theta}}_{\boldsymbol{i}}$ to the right-hand side of (13.70) yields

$$\dot{V}_2 \leq -\sigma_2 V_2 + \rho_2, \tag{13.71}$$

where

$$\begin{aligned}\sigma_2 &= \min\left(1, \frac{2(c_1+d_{11})}{m_{11}^{\min}}\right),\\ \rho_2 &= \frac{1}{2}\sum_{i=1}^{2}\tilde{\boldsymbol{\theta}}_{\boldsymbol{i}}^{\boldsymbol{T}}\boldsymbol{\Gamma}_{\boldsymbol{i}}^{-\mathbf{1}}\tilde{\boldsymbol{\theta}}_{\boldsymbol{i}} + 0.2785\sum_{i=1}^{3}\varepsilon_{2i},\end{aligned} \tag{13.72}$$

with $m_{11}^{\min}$ being the minimum value of m_{11}. From (13.71), it is direct to show that

$$V_2(t) \leq V_2(t_0)e^{-\sigma_2(t-t_0)} + \frac{\rho_2}{\sigma_2}, \tag{13.73}$$

which further yields

$$|\tilde{u}(t)| \leq \sqrt{2V_2(t_0)}e^{-\sigma_2/2(t-t_0)} + \sqrt{\frac{2\rho_2}{\sigma_2}} := \alpha_u(\cdot)e^{-\sigma_2/2(t-t_0)} + \rho_u. \tag{13.74}$$

Remark 13.3. It is noted that, due to the use of the projection algorithm, by adjusting $\boldsymbol{K_2}$, $\boldsymbol{K_3}$, c_1, ε_{2i}, ε_{4i}, γ_{1j}, γ_{2i}, γ_{3n}, γ_{4l}, $1 \leq i \leq 3$, $1 \leq j \leq 16$, $1 \leq n \leq m_3$, and $1 \leq l \leq m_4$, we can make ρ_u, ρ_η and ρ_v arbitrarily small. This observation plays an important role in the stability analysis of the d_e-dynamics.

d_e-dynamics. We first calculate the lower-bound of d_e. We now show that there exist initial conditions such that $d_e(t) \geq d_e^* > 0$. From (13.46) and (13.16), we have

$$\dot{\tilde{d}}_e \geq -k_1\tilde{d}_e - \left(\alpha_u e^{-\sigma_2/2(t-t_0)} + \rho_u\right), \tag{13.75}$$

where $\tilde{d}_e = d_e - \delta_e$, which with $\sigma_2 > 2k_1$ further yields

$$\begin{aligned}\tilde{d}_e(t) \geq\ & \tilde{d}_e(t_0)e^{-k_1(t-t_0)} + \frac{\alpha_u(\cdot)e^{-k_1(t-t_0)}}{\sigma_2/2-k_1}\left(-1+e^{-(\sigma_2/2-k_1)(t-t_0)}\right) -\\ & \frac{\rho_u}{k_1}\left(1-e^{-k_1(t-t_0)}\right).\end{aligned} \tag{13.76}$$

Therefore, the condition $d_e(t) \geq d_e^* > 0$ holds when

$$\sigma_2 > 2k_1,\ \delta_e \geq d_e^* + \frac{\rho_u}{k_1}, d_e(t_0) \geq \frac{\alpha_u(\cdot)}{\sigma_2/2-k_1} + \delta_e - \rho_u. \tag{13.77}$$

We will come back to this issue in the next section. We now calculate the upper-bound of d_e. We rewrite (13.46) as

$$\dot{\tilde{d}}_e = -k_1\tilde{d}_e - \cos(\gamma)\tilde{u} - k_1\left(\cos(\gamma_1)-1\right) + \cos(\gamma)(\cos(\gamma_2)-1))\,\tilde{d}_e. \quad (13.78)$$

Since (13.78) and the $(\tilde{u}, \gamma_1, \gamma_2)$-subsystem are in the cascade form, one might think that the stability results developed for cascade systems in [17] and [69] can be applied. However, the stability results in those papers were developed for cascade systems without nonvanishing disturbances. In fact, nonvanishing disturbances may destroy the stability of a cascade system that satisfies all conditions stated in the above papers. Therefore, we will use Lemma 10.1 to investigate the stability of the system (13.78) by verifying all conditions C1–C4.

Verifying Condition C1. Take the Lyapunov function

$$V_3 = \frac{1}{2}d_e^2. \quad (13.79)$$

It is direct to show that C1 holds with

$$c_0 = 0, c_1 = c_2 = 0.5, c_3 = 1, c_4 = k_1. \quad (13.80)$$

Verifying Condition C2. By noting that

$$\left|\cos(\gamma)\tilde{u} + k_1\left(\cos(\gamma_1)-1\right) + \cos(\gamma)(\cos(\gamma_2)-1))\,\tilde{d}_e\right| \leq |\tilde{u}| + k_1\left(|\gamma_1| + |\gamma_2|\right)\left|\tilde{d}_e\right|, \quad (13.81)$$

we have

$$\lambda_1 = 1,\ \lambda_2 = k_1. \quad (13.82)$$

Verifying Condition C3. This condition directly holds from (13.74) and (13.68).

Verifying Condition C4. From (13.80) and (13.82), condition C4 becomes

$$k_1 - \max(\rho_\eta, \rho_u)\left(k_1 + 0.25\mu_0\right) > 0. \quad (13.83)$$

From Remark 13.3 and noting that μ_0 is an arbitrarily positive constant, we can see that there always exists k_1 such that (13.83) holds. All conditions of Lemma 10.1 have been verified, and we therefore have

$$|d_e(t)| \leq \alpha_{de}(\cdot)\, e^{-\sigma_{de}(t-t_0)} + \rho_{de}, \quad (13.84)$$

where α_{de}, σ_{de} and ρ_{de} are calculated as in Lemma 10.1.

(v, w)-dynamics. Expanding (13.55) gives

$$\begin{aligned} q_d = \ & -\left(J_2^{21}(\boldsymbol{\eta_2})k_{21}\phi + J_2^{22}(\boldsymbol{\eta_2})k_{22}\gamma_1 + J_2^{23}(\boldsymbol{\eta_2})k_{23}\gamma_2\right) - \\ & J_2^{22}(\boldsymbol{\eta_2})\left(f_1^s\dot{s} + f_1^u u\right) - J_2^{23}(\boldsymbol{\eta_2})\left(f_2^s\dot{s} + f_2^u u\right) - \\ & \left(J_2^{22}(\boldsymbol{\eta_2})f_1^v + J_2^{23}(\boldsymbol{\eta_2})f_2^v\right)v - \left(J_2^{22}(\boldsymbol{\eta_2})f_1^w + J_2^{23}(\boldsymbol{\eta_2})f_2^w\right)w, \end{aligned}$$

$$\begin{aligned} r_d = & -\left(J_2^{31}(\boldsymbol{\eta_2})k_{21}\phi + J_2^{32}(\boldsymbol{\eta_2})k_{22}\gamma_1 + J_2^{33}(\boldsymbol{\eta_2})k_{23}\gamma_2\right) - \\ & J_2^{32}(\boldsymbol{\eta_2})\left(f_1^s\dot{s} + f_1^u u\right) - J_2^{33}(\boldsymbol{\eta_2})\left(f_2^s\dot{s} + f_2^u u\right) - \\ & \left(J_2^{32}(\boldsymbol{\eta_2})f_1^v + J_2^{33}(\boldsymbol{\eta_2})f_2^v\right)v - \left(J_2^{33}(\boldsymbol{\eta_2})f_1^w + J_2^{33}(\boldsymbol{\eta_2})f_2^w\right)w, \end{aligned} \tag{13.85}$$

where $J_2^{ij}(\boldsymbol{\eta_2})$ is the element at the ith row and jth of $\boldsymbol{J_2^{-1}}(\boldsymbol{\eta_2})$. To show that the sway and heave velocities are bounded, we take the following quadratic function

$$V_4 = \frac{1}{2}m_{22}^2 v^2 + \frac{1}{2}m_{33}^2 w^2, \tag{13.86}$$

whose derivative along (13.37), (13.54), and (13.85) satisfies

$$\begin{aligned} \dot{V}_4 \leq & -m_{22}d_{v3}v^4 - m_{33}d_{w2}|w|w^2 - m_{33}d_{w3}w^4 + A_3^{\max}v^2 + A_4^{\max}w^2 + \\ & \frac{1}{4\varepsilon_5}A_1^{\max} + \frac{1}{4\varepsilon_6}A_2^{\max}, \end{aligned} \tag{13.87}$$

where $\varepsilon_i > 0, i = 1,2$, $A_j^{\max}, 1 \leq j \leq 4$ is the maximum value of A_j with

$$\begin{aligned} A_1 = & -m_{11}m_{22}u\left(\tilde{r} - J_2^{31}(\boldsymbol{\eta_2})k_{21}\phi - J_2^{32}(\boldsymbol{\eta_2})k_{22}\gamma_1 - J_2^{33}(\boldsymbol{\eta_2})k_{23}\gamma_2 - \right. \\ & \left. J_2^{32}(\boldsymbol{\eta_2})\left(f_1^s\dot{s} + f_1^u u\right) - J_2^{33}(\boldsymbol{\eta_2})\left(f_2^s\dot{s} + f_2^u u\right)\right) + m_{22}\tau_{wv(t)}, \\ A_2 = & \; m_{11}m_{33}u\left(\tilde{q} - J_2^{21}(\boldsymbol{\eta_2})k_{21}\phi - J_2^{22}(\boldsymbol{\eta_2})k_{22}\gamma_1 - J_2^{23}(\boldsymbol{\eta_2})k_{23}\gamma_2 - \right. \\ & \left. J_2^{22}(\boldsymbol{\eta_2})\left(f_1^s\dot{s} + f_1^u u\right) - J_2^{23}(\boldsymbol{\eta_2})\left(f_2^s\dot{s} + f_2^u u\right)\right) + m_{33}\tau_{ww(t)}, \\ A_3 = & \left(-m_{22}d_{22} - m_{22}d_{v2}|v| + \varepsilon_5|A_1| + \frac{m_{11}m_{22}\left|uJ_2^{33}(\boldsymbol{\eta_2})\left(f_1^w + f_2^w\right)\right|}{2} + \right. \\ & \left. \frac{m_{11}m_{33}\left|uJ_2^{22}(\boldsymbol{\eta_2})\left(f_1^v + f_2^v\right)\right|}{2}\right), \\ A_4 = & \left(-m_{33}d_{33} - m_{33}d_{w2}|w| + \varepsilon_6|A_2| + \frac{m_{11}m_{22}\left|uJ_2^{33}(\boldsymbol{\eta_2})\left(f_1^w + f_2^w\right)\right|}{2} + \right. \\ & \left. \frac{m_{11}m_{33}\left|uJ_2^{22}(\boldsymbol{\eta_2})\left(f_1^v + f_2^v\right)\right|}{2}\right). \end{aligned} \tag{13.88}$$

It can be seen from (13.88) that $A_i^{\max}$ exist and are finite since their arguments are bounded as shown above. Hence (13.87) and (13.86) guarantee a finite upper bound of the sway and heave velocities.

Initial Conditions for $|\gamma(t)| < \frac{\pi}{2}$, $|\gamma_i(t)| < \frac{\pi}{2}, i = 1,2, \forall t \geq t_0 \geq 0$. Since $|\gamma_i(t)| \leq \left\|\boldsymbol{\eta}_{2\gamma}(t)\right\|$, $i = 1,2,\ \forall t \geq t_0 \geq 0$, from (13.68), it is direct to show that the condition $|\gamma_i(t)| < 0.5\pi$, $i = 1,2,\ \forall t \geq t_0 \geq 0$ holds if the initial conditions are such that

$$\sqrt{2V_1(t_0)} + \sqrt{2\rho_1/\sigma_1} < 0.5\pi, \tag{13.89}$$

which is further equivalent to

$$\sqrt{\left\|\eta_{2\gamma}(t_0)\right\|^2 + \lambda_{\max}(M_2)\left\|\tilde{v}_2(t_0)\right\|^2 + \sum_{i=1}^{4}\Gamma_i^{-1}\left\|\tilde{\theta}_i(t_0)\right\|^2} + \sqrt{2\frac{\rho_1}{\sigma_1}} < \frac{\pi}{2}, \quad (13.90)$$

for all $t \geq t_0 \geq 0$. It is noted that the terms $\sum_{i=1}^{4}\boldsymbol{\Gamma}_i^{-1}\left\|\tilde{\boldsymbol{\theta}}_i(t_0)\right\|^2$ and ρ_1 can be made arbitrarily small, see Remark 13.3.

From (13.33) and (13.16), the condition $|\gamma(t)| < 0.5\pi$, $\forall t \geq t_0 \geq 0$ holds if the initial conditions are such that

$$\cos(\gamma_1(t)) + \frac{a_e(t)}{d_e(t)}\cos(\theta(t))(\cos(\gamma_2(t) - 1) > 0. \quad (13.91)$$

Under the assumption that $|\theta(t)| < 0.5\pi$, $\forall t \geq t_0 \geq 0$, the above condition is equivalent to

$$\cos(\gamma_1(t)) + \cos(\gamma_2(t)) > 1. \quad (13.92)$$

From (13.68), the condition (13.92) holds if the initial conditions are such that

$$\sqrt{\left\|\boldsymbol{\eta_{2\gamma}}(t_0)\right\|^2 + \lambda_{\max}(\boldsymbol{M_2})\left\|\tilde{\boldsymbol{v}}_{\boldsymbol{2}}(t_0)\right\|^2 + \sum_{i=1}^{4}\boldsymbol{\Gamma_i^{-1}}\left\|\tilde{\boldsymbol{\theta}}_{\boldsymbol{i}}(t_0)\right\|^2} + \sqrt{2\frac{\rho_1}{\sigma_1}} < \arccos(0.5), \ \forall t \geq t_0 \geq 0. \quad (13.93)$$

Since $\arccos(0.5) < 0.5\pi$, the condition (13.93) covers the condition (13.90).

Initial Conditions for $a_e(t) \geq a_e^* > 0$, $\forall t \geq t_0 \geq 0$. Since $a_e^2 = d_e^2 - z_e^2$, we have

$$\begin{aligned}\dot{a_e^2} &= 2\left(d_e\left(-k_1\cos(\gamma)d_e + k_1\cos(\gamma)\delta_e - \cos(\gamma)\tilde{u}\right) - \right.\\ &\quad \left. z_e\left(\frac{\partial z_d}{\partial s}\dot{s} + \sin(\theta)u - \cos(\theta)\sin(\phi)v - \cos(\theta)\cos(\phi)w\right)\right)\\ &= -2k_1\cos(\gamma)a_e^2 + 2k_1\cos(\gamma)z_e^2 + 2k_1\cos(\gamma)d_e\delta_e - 2\cos(\gamma)d_e\tilde{u} -\\ &\quad 2z_e\left(\frac{\partial z_d}{\partial s}\dot{s} + \sin(\theta)u - \cos(\theta)\sin(\phi)v - \cos(\theta)\cos(\phi)w\right). \quad (13.94)\end{aligned}$$

From (13.94), it is not hard to see that under Assumption 13.1 and $d_e(t) \geq d_e^* > 0$, if there exists a strictly positive constant a_e^0 such that

$$a_e(t_0) \geq a_e^0, \quad (13.95)$$

then there exists a strictly positive constant a_e^* such that the condition $a_e(t) \geq a_e^* > 0$, $\forall t \geq t_0 \geq 0$ holds.

In summary, the feasible initial conditions are such that the conditions (13.77), (13.93) and (13.95) hold. Roughly speaking, with the above initial conditions, due to the underactuated configuration in the sway and heave, the sway and heave velocities are not able to push the vehicle to the point $a_e = 0$ and $d_e = 0$.

13.5 Discussion of the Initial Condition

We now discuss how to obtain the initial conditions such that (13.77), (13.93), and (13.95) hold. A close look at these conditions shows that they are always satisfied by selecting the initial value, $s(t_0)$, if the vessel heads toward the conical space containing the initial path to be followed, see Figure 13.2. If the vessel does not, the surge control should be turned off and the yaw and pitch controls should make the vessel turn until (13.77), (13.93), and (13.95) hold before applying the proposed path-following controller. The angle δ_0 (see Figure 13.2) should be increased if the initial velocities $\boldsymbol{v_1}(t_0)$ and $\boldsymbol{v_2}(t_0)$ are large. Otherwise the vessel might cross the edge-line of the subspace in question, which might result in $\gamma_i = \pm 0.5\pi$ and/or $\gamma = \pm 0.5\pi$.

13.6 Parking and Point-to-point Navigation

13.6.1 Parking

Parking Objective. Design the controls $\boldsymbol{\tau_1}$ and $\boldsymbol{\tau_2}$ to park the underactuated underwater vehicle (13.1) from the initial position and orientation $(x(t_0), y(t_0), z(t_0), \phi(t_0), \theta(t_0), \psi(t_0))$ to the desired parking position and orientation of $(x_p, y_p, z_p, \phi_p, \theta_p, \psi_p)$ under the following conditions:

1. There exists a large enough positive constant ϖ_p such that

$$\sqrt{\big(x(t_0)-x_p\big)^2+\big(y(t_0)-y_p\big)^2+\big(z(t_0)-z_p\big)^2} \geq \varpi_p.$$

2. The vessel heads toward the feasible cone containing the desired parking orientation, see Section 13.5.
3. At the desired parking position and orientation, the environmental disturbances are negligible.

The above conditions normally hold for parking practice. However, if the first two conditions do not hold, one can apply the strategy in Section 13.5 to move the vessel until they do hold. Having formulated the parking problem as above, one might claim that the path-following controller proposed in Section 13.3 can be applied by setting u_0 equal zero. However, this will result in an orientation that may be very different from the desired parking one, at the desired parking position, since

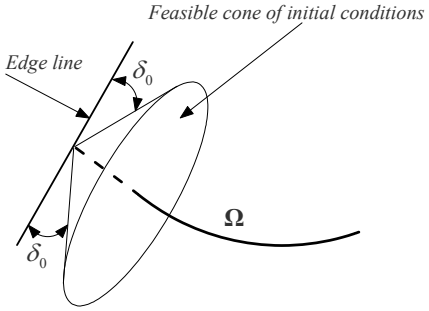

Figure 13.2 Feasible initial conditions

our proposed path-following controller is designed to drive d_e to a small ball, not to zero for reasons of robustness. To resolve this problem, we first generate a regular curve, $\boldsymbol{\Omega_p}(x_d, y_d, z_d)$, which goes via the parking position and its orientation at the parking position is equal to the desired parking condition. For simplicity of calculation, the curve can be taken as a straight line in almost all cases of the vessel's initial conditions. Then the proposed path-following controller can be used to make the vessel follow $\boldsymbol{\Omega_p}(x_d, y_d, z_d)$. In this case, the velocity u_0 should be chosen such that it goes to zero when the virtual vessel tends to the desired parking position, i.e., $\lim_{d_{ep}\to 0} u_0 = 0$ with $\mathrm{d}_{ep} = \sqrt{(x_d - x_p)^2 + (y_d - y_p)^2 + (z_d - z_p)^2}$. A simple choice can be taken as

$$u_0 = u_0^*(1 - e^{-\chi_1 d_{ep}})e^{-\chi_2 d_e}, \tag{13.96}$$

where $\chi_i > 0, i = 1, 2$. Special care should be taken to choose the initial values of $(x_d(t_0), y_d(t_0), z_d(t_0))$, see Section 13.5, and the sign of u_0 such that it results in a short parking time.

Remark 13.4. Once at the desired parking position and orientation, if there are large environmental disturbances, there will be an oscillatory behavior in the yaw and pitch dynamics, and the vessel might diverge from its desired position. This phenomenon is well known in ship dynamic positioning.

13.6.2 Point-to-point Navigation

As seen in Section 13.1, the requirement that the reference path be a regular curve might be too cumbersome in practice, since this curve has to go via desired points generated by the helmsman and its derivatives are needed in the path-following controller. These restrictions motivate us to consider the point-to-point navigation problem as follows.

Point-to-point Navigation Objective. Design the surge force $\boldsymbol{\tau_u}$ and the yaw moment $\boldsymbol{\tau_r}$ to force the underactuated underwater vehicle (13.1) from the initial position and orientation, $(x(t_0), y(t_0), z(t_0), \phi(t_0), \theta(t_0), \psi(t_0))$, to go via the desired points generated by a path planner.

To achieve this control objective, we first assume that the path planner generates desired points, which are feasible for the vehicle to be navigated through. We then apply the path-following controller proposed in Section 13.3 to each regular curve segments connecting desired points in sequence. The regular curve segments can be straight line, arc, or known regular curve ones. It is, however, noted that a fundamental difference between point-to-point navigation and the proposed smooth path-following is that there are a finite number of "peaks", equal to the number of points, in the orientation errors, γ_1 and γ_2. This phenomenon is because the path is non-smooth in the orientation at the points.

13.7 Numerical Simulations

This section validates the control laws (13.48) and (13.59) by simulating them on a 5.56 m long underwater vehicle whose parameters are given in Section 12.5. The values of the vehicle parameters are assumed to be of the real vessel and are estimated on-line by the adaptation laws (13.49) and (13.60). We assume that these parameters fluctuate around the above values $\pm 15\%$. This fluctuation is chosen here for the purpose of calculating the maximum and minimum values used in the choice of the design constants. Indeed, a different fluctuation of the vehicle parameters results in different maximum and minimum values used in the choice of the design constants. In the simulation, we assume that the environmental disturbances are

$$\tau_{wu} = 0.2m_{11}d(t),\ \tau_{wv} = 0.2m_{22}d(t),\ \tau_{ww} = 0.2m_{33}d(t),\ \tau_{wp} = 0.2m_{44}d(t),$$
$$\tau_{wq} = 0.2m_{55}d(t),\ \tau_{wr} = 0.2m_{66}d(t),$$

where $d(t) = 1 + 0.1\sin(0.2t)$. This choice results in nonzero-mean disturbances. In practice, the environmental disturbances may be different. We take the above disturbances for an illustration of the robustness properties of our proposed controller. It should be noted that only upper bounds of the environmental disturbances are needed in our proposed controller.

In the simulation, based on Section 13.3 the control parameters and initial conditions are taken as

$$k_1 = 0.5, c_1 = 2,\ \boldsymbol{K_2} = \mathrm{diag}(0.05),\ \boldsymbol{K_3} = \mathrm{diag}(2), \boldsymbol{\Gamma_i} = \mathrm{diag}(10),\ \delta_e = 0.2,$$
$$\left[\boldsymbol{\eta_1}^T(t_0), \boldsymbol{\eta_2}^T(t_0), \boldsymbol{v_1}^T(t_0), \boldsymbol{v_2}^T(t_0), s(t_0)\right]^T =$$
$$[-145, -15, -5, 0, 0.2, 0.5, 0, 0, 0, 0, 0, 0, 0]^T,$$

and all initial values of parameter estimates are taken to be 70% of their assumed true ones. The virtual vessel velocity on the path is taken as $u_0(t, d_e) = 5(1 - 0.8e^{-2t})e^{-0.5d_e}$. The reference path is given by ($x_d = -90\cos(s)$, $y_d =$

$90\sin(s), z_d = 3s$), i.e., a helix with constant curvature and torsion. Figure 13.3 plots the trajectory of the vessel and the path (dotted line) to be followed in three dimensions. The trajectory of the vessel in the horizontal plane and the path following error are plotted in Figure 13.4. Figure 13.5 plots the control inputs, τ_u, τ_r, τ_p, and τ_q. With nonvanishing environmental disturbances, our proposed controller is able to force the vehicle to follow a predefined path as expected in the control design. As can be seen in Figure 13.5, d_e converges to a nonzero small value, i.e., the sway and heave velocities cannot push the vessel to the point where $d_e = 0$. From Figure 13.5, it can be seen that the control inputs are below their limits. Therefore, we can still further shorten the transient time by increasing the control gains.

13.8 Conclusions

The control scheme developed for path-following of underactuated surface ships in Chapter 11 was extended to design a path-following system for six degrees of freedom underactuated underwater vehicles. The key to the development of the proposed path-following system is the proper selection of the coordinate transformations in Section 13.2. The work presented in this chapter is based on [140, 141].

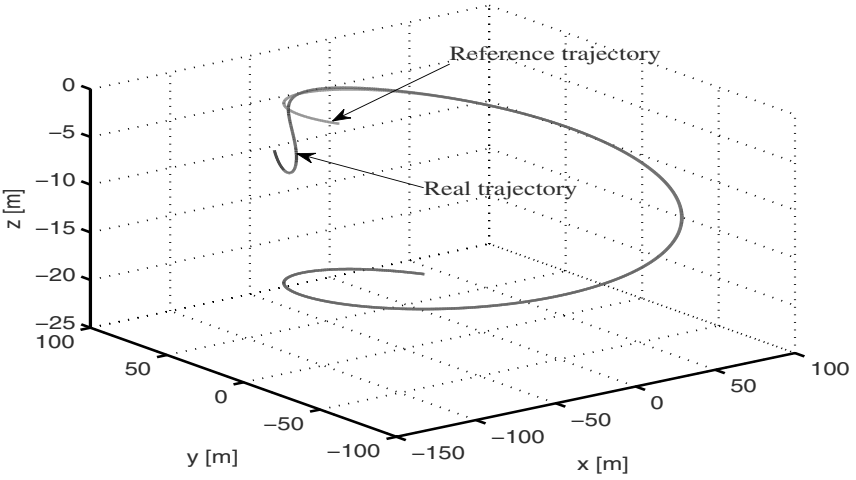

Figure 13.3 Simulation results: Path-following real and reference trajectories in three-dimensional space

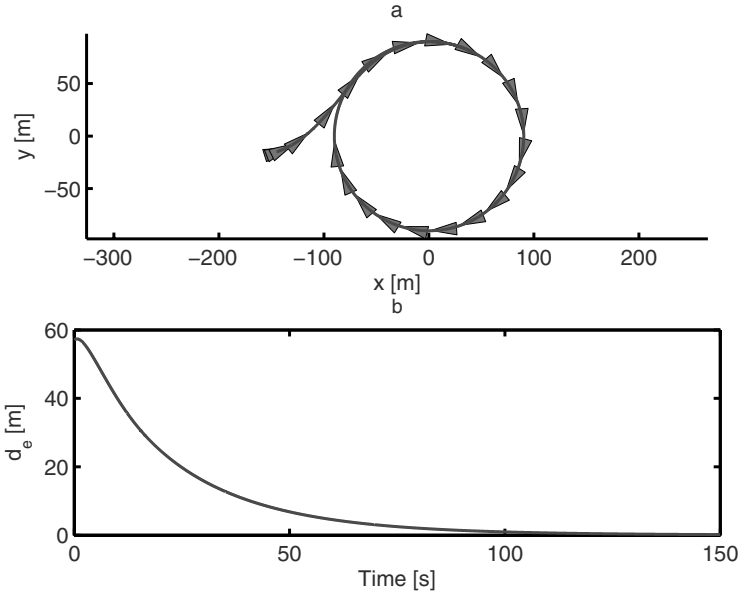

Figure 13.4 Simulation results: **a**. Path-following trajectory in the horizontal plane; **b**. Path-following error d_e

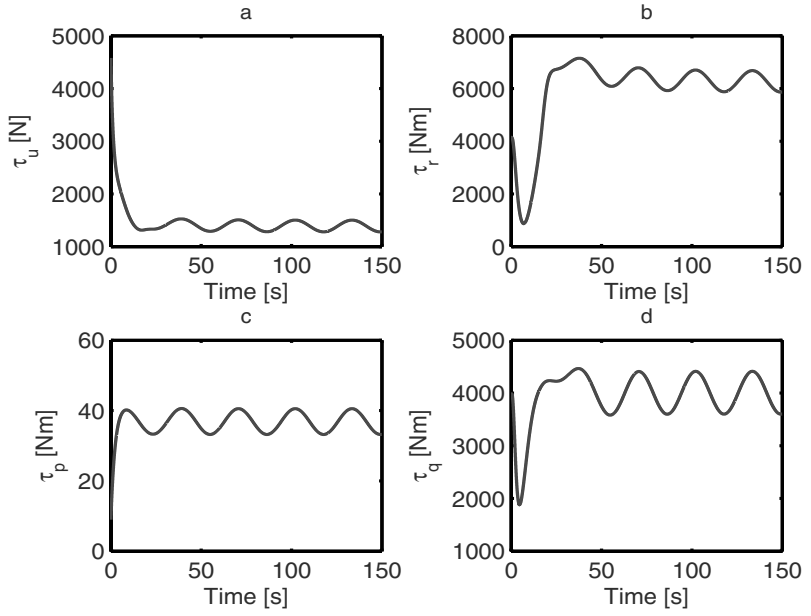

Figure 13.5 Simulation results (control inputs): **a**. Surge force τ_u [N]; **b**. Yaw moment τ_r [Nm]; **c**. Pitch moment τ_p [Nm]; **d**. Roll moment τ_q [Nm]